Catalysis Today 243 (2015) 235–250

Contents lists available at ScienceDirect

Catalysis Today

journal homepage: www.elsevier.com/locate/cattod

Fate of methanol under one-pot artificial photosynthesis condition with metal-loaded TiO_2 as photocatalysts

Agni Raj Koirala, Son Docao, Seong Beom Lee, Kyung Byung Yoon *

Korea Center for Artificial Photosynthesis, Center for Nanomaterials, Program of Integrated Biotechnology, Department of Chemistry, Sogang University, Seoul 121-742, Republic of Korea

ARTICLE INFO

Article history:
Received 23 June 2014
Received in revised form 18 July 2014
Accepted 24 July 2014
Available online 26 September 2014

Keywords:
Artificial photosynthesis
Photocatalytic dehydrogenation
Methanol steam reforming
Formaldehyde autooxidation
Oxidative coupling
Charge transfer

ABSTRACT

The experimental artificial photosynthesis (AP) systems, which have attempted AP by photo-irradiation of single-chamber reactors containing CO_2, H_2O, and metal-loaded TiO_2, have received great attention during the last three decades. Such one-pot AP systems cannot be efficient because the catalysts have water oxidation sites which can oxidize the carbon-containing organic fuels more readily than water. Despite this, methanol has been the most desired product from such AP systems due to its many merits. However, CH_4 and CO have been produced as major products under normal conditions (1 bar of CO_2, 1 sun, neutral condition, and irradiation wavelength > 350 nm). From a systematic study aimed to elucidate the fate of methanol in such one-pot AP systems with novel metal nanoparticle loaded TiO_2 (M_n–TiO_2, M = Pd, Pt, Cu and Au) as the catalyst we found that methanol and its related products formaldehyde and formic acid are not produced from such one-pot AP systems, indicating that the gaseous products should be produced from the pathways which do not involve methanol and the less-reduced products as intermediates or side products. We also elucidated that when methanol is added into the AP system, as many as fifteen different reactions take place as shown in Scheme 1. The reaction is initiated by photoinduced excitation of the charge-transfer (CT) band from methanol to TiO_2 surface, which appears in the UV region, by the UV part of the solar light. These reactions bear the potential to be used for production of various compounds.

1. Introduction

Artificial photosynthesis (AP), namely, the sun light driven conversion of carbon dioxide (CO_2) and water into fuel, is currently an important area of research [1–53]. The most desired target product from AP has been methanol (CH_3OH) because it exists in the liquid form under the ambient condition and can be transformed into various useful compounds. Since methanol is a $6e^-$-reduced product of CO_2, the simultaneous formation of formaldehyde (HCHO, $4e^-$-reduced product) and formic acid (HCOOH, $2e^-$-reduced product) is also likely if an AP system produces methanol.

The simplest approach to materialize AP is to charge a single chamber reactor with CO_2, water, and a proper photocatalyst, and subsequently irradiate the reactor with a proper light source or expose it to the sun light. This so-called 'one-pot' approach for AP has been experimented by a large number of groups for more than three decades [18–53]. For this approach, the TiO_2 powders loaded with various metal nanoparticles (M_n–TiO_2) have been extensively tested as photocatalysts [18–40,44–53]. However, under the normal condition (1 bar of CO_2, neutral solution, and 1 sun) only gaseous products such as methane (CH_4) and carbon monoxide (CO) have been the major products and CH_3OH and the less reduced products have not been produced unless the reactions were carried out under extreme conditions which involve very high CO_2 pressures (10–75 bar) [34–36], highly basic solution (pH > 13) [37–39], very high intensities of sun light (20–100 sun) [40], or with UV lights with the wavelengths shorter than 350 nm [18,21–26,44,46,48,51]. However, molecular hydrogen (H_2) has never been detected from such one-pot AP systems with M_n–TiO_2 as photocatalysts.

To explain the reasons for the formation of methane as the most common product [19], three pathways called formaldehyde pathway [44,45], carbene pathway [20a,46–50], and glyoxal pathway [51–53] have been proposed. However, these pathways involve formic acid, formaldehyde, or methanol as a key intermediate or a side product. In fact, it is quite unreasonable to expect CH_3OH and the less reduced products from the one-pot AP systems because they carry both water oxidation site as well as CO_2 reduction site. Thus, if the former could oxidize water, then it surely can oxidize

* Corresponding author. Tel.: +82 10 4041 6799; fax: +82 2 706 4269.
E-mail address: yoonkb@sogang.ac.kr (K.B. Yoon).

http://dx.doi.org/10.1016/j.cattod.2014.07.056
0920-5861/

CH_3OH, HCHO, and HCOOH much more readily than water because these organic compounds are better electron donors than water. M_n–TiO_2 has also been extensively used as the environmental photooxidation catalysts for removal of HCHO [54] and various organic molecules in the air and in water [55–65]. In this respect, the one-pot AP systems, in particular those with M_n–TiO_2 as photocatalysts, should be viewed as 'unideal' AP systems.

Now the following fundamental questions arise. Would such AP systems indeed be able to produce CH_3OH, HCHO, and HCOOH? Regardless of the answer to the previous question, what would happen to CH_3OH and the less reduced products if they were deliberately introduced into such one-pot AP systems? Would CH_4 and CO be produced from CH_3OH and the less reduced products during the course of their decomposition under the one-pot AP condition? If not, from where would they come? Then what happens to the proposed three pathways? Are there independent pathways for the formation of CH_4 and CO under the one-pot AP conditions?

The answers to the above questions will help us better understand the problems of the one-pot AP systems. They will also give us valuable information regarding the fates of CH_3OH and the less reduced products in such one-pot AP systems. They will also help us find the important clues on how CH_4 and CO become produced from such AP systems. Thus, the answers to the above questions will eventually give us valuable insights into the design of efficient AP systems.

With the above background in mind we have conducted a series of photocatalytic oxidation of CH_3OH and its less reduced products on several metal oxide nanoparticle-loaded TiO_2 [$(MO)_n$–TiO_2, M = Pd, Pt, Au, and Cu] by feeding the reactant vapors, as a single component or as a mixture, with or without the water vapor, into the reactor charged with $(MO)_n$–TiO_2 powder. Here, the reason why we used $(MO)_n$–TiO_2 as photocatalysts instead of M_n–TiO_2 is because we later found that $(MO)_n$–TiO_2 are first converted to M_n–TiO_2 (*vide infra*) under the reaction condition (for M = Pd, Pt, and Cu) or during the catalyst preparation (for M = Au). Thus, the use of $(MO)_n$–TiO_2 is a more convenient way to carry out the reaction.

CO_2 was also fed into the reactor as the carrier gas as a means to provide an AP condition. However, we also carried out the photocatalytic oxidation with Ar as the carrier gas to investigate the possibility of CH_3OH and less reduced products to form CO_2. Since one-pot AP systems also produce molecular oxygen, O_2, through water oxidation, all the photocatalytic reactions should also undergo under the O_2 environment. In this regard, we also used O_2 as the carrier gas. Another reason for using O_2 as a carrier gas was to investigate the effect of an oxidizing carrier gas on the pathways of photooxidation of CH_3OH and the less reduced products on M_n–TiO_2. We also used H_2 as a carrier gas to investigate the effect of a reducing carrier gas on the pathways of photooxidation of CH_3OH and the less reduced products on M_n–TiO_2. Thus, we have investigated the photocatalytic oxidation of CH_3OH, HCHO, and HCOOH, under the four different carrier gas conditions.

The reason we carried out the above photocatalytic oxidation reactions under the vapor–solid heterogeneous condition is to facilitate the quantitative analyses of the products by feeding the product stream on-line into one or two gas chromatographs (GCs) and to a gas chromatograph-mass spectrometer (GC–MS) and to investigate the effect of methanol-to-water molar ratio ($0.1–\infty$) on the pathways of the photocatalytic oxidation of the reactant molecules and on the product distributions.

We now report that the one-pot AP systems with M_n–TiO_2 as photocatalysts do not produce CH_3OH, HCHO, and HCOOH, and accordingly, the CH_4 and CO which have been routinely observed as the major products from the one-pot AP systems in the literature [1,8b,14,16b,21a,23–29,31–33,41,43–45,49,53] do not come from photocatalytic oxidation of CH_3OH, HCHO, and HCOOH. Thus, this report raises strong doubts onto the three pathways that have been proposed for the formation of methane as the major product from the one-pot AP systems. We also report the remarkable fact that while HCHO and HCOOH simply undergo decomposition to H_2 and CO_2 in the moist atmosphere, CH_3OH leads to formation of various products such as HCHO, dihydoxymethane or methane diol $H_2C(OH)_2$, HCOOH, methyl formate (MF) HCO_2CH_3, methoxy methanol CH_3OCH_2OH, dimethoxy methane (DMM) $(CH_3O)_2CH_2$, dimethyl ether (DME) CH_3OCH_3, CH_4, CO_2, CO, H_2, and H_2O by involving as many as fifteen different reactions (Scheme 1). We further report the characteristic features of the fifteen reactions, their flow, their relationships, their relative rates, and the effect of carrier gas on each reaction and the reaction pathways, the effects of methanol-to-water (M/W), formaldehyde-to-methanol (F/M), and MF-to-water (MF/W) ratios, respectively, on the corresponding product distribution and reaction pathway.

2. Experimental

2.1. Materials

TiO_2 (P25) was purchased from Degussa. Copper acetate monohydrate [$Cu(CH_3COOH)_2{\cdot}H_2O$], palladium(II) chloride ($PdCl_2$), platinum(II) chloride ($PtCl_2$), gold(III) chloride trihydrate ($HAuCl_4{\cdot}xH_2O$), an aqueous formaldehyde solution, an aqueous formic acid were purchased from Aldrich and used as received. Anhydrous methanol, anhydrous methyl formate, and anhydrous 1,1-dimethoxymethane [$(CH_3O)_2CH_2$] were purchased from Aldrich and further dried by immersing them, respectively, in dried 13X zeolite pellets, in a glove box, and used after filtration of the 13X zeolite pellets.

2.2. Instrumentation

Diffuse-reflectance UV–vis spectra of the samples were recorded on a Varian Cary 5000 UV–vis–NIR spectrometer equipped with an integrating sphere. Barium sulfate was used as the reference. The diffuse reflectance spectra were converted into the Kubelka–Munk function (K–M). The gas chromatographs were purchased from Young Lin (YL-6000) equipped with a thermal conductivity detector, a flame ionization detector (FID), a methanizer, and a pulsed discharged detector (PDD). GC–MS was from Perkin Elmer Clarus 600 GC and Clarus 600 T-mass spectrometer. Transmission electron microscopy (TEM) images were collected on a JEOL JEM 4010 microscope.

2.3. Reaction procedure

Each $(MO)_n$–TiO_2 powder (350 mg) was spread at the bottom of a reactor having a quartz window at the top. The temperature of the reactor was maintained at 30 °C. The reactants were fed into the reactor in the vapor phase, as a single component or as a mixture of two components, by passing a carrier gas through a bubbler filled with a single component or a mixture of two components. To study the effect of moisture on the reaction, reactants and catalysts were kept under both the anhydrous and moist conditions, respectively. A carrier gas was chosen from CO_2, Ar, H_2, and O_2 and the flow rate was kept at 6 mL min^{-1} using a mass flow controller. The flow rate was calibrated using a bubble flow meter. The amount of reactant vapor in the gas stream was controlled by controlling the temperature of the bubbler. The reactor was first flushed with Ar (99.9999%) for variable periods of time to remove air and the residual products from the previous reactions. Each reaction was carried out in the dark and under the photoirradiation condition, respectively, in the presence and absence of a catalyst, respectively, to investigate each reaction under the photocatalytic, non-catalytic photo, thermocatalytic, and non-catalytic thermal conditions, respectively. For

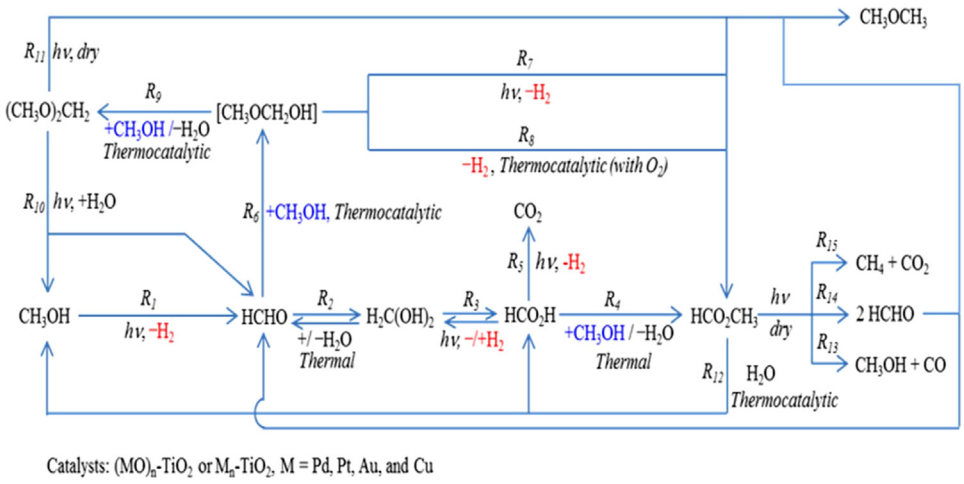

Scheme 1. The flow and interconnectivity of diverse reactions that take place during vapor phase photocatalytic oxidation of methanol in the presence and absence of water on metal oxide nanoparticles $(MO)_n$ supported on TiO_2 and their characteristics ((M_n = Pd_n, Pt_n, Au_n, and Cu_n).

photoreactions, a standard AM-1.5 solar simulated light (HAL-302 Asahi) with the power of 72 mW cm^{-2} was used. The intensity of the light was adjusted using a 1-sun checker (CS-20, Asahi Spectra Co., Ltd.). The area of irradiation was 6 cm^2. The amounts of introduced reactants and products are reported in terms of μmol per unit area (1 cm^2) per h (μmol cm^{-2} h^{-1}).

2.4. Preparation of $Pd(NH_3)_4Cl_2$ and $Pt(NH_3)_4Cl_2$

$PdCl_2$ and $PtCl_2$ were converted to the corresponding tetramine complex by reacting them with dry ammonia, respectively, according to the known procedure [66]. Typically, 2 g of $PdCl_2$ was introduced into a two-neck round bottomed flask and NH_3 gas was passed through the flask until the dark gray color of $PdCl_2$ changed to white. The same procedure was carried out for the preparation of $Pt(NH_3)_4Cl_2$.

2.5. Preparation of $(MO)_n$–TiO_2

P25 (3 g) and a calculated amount of a metal precursor [$Cu(CH_3COOH)_2{\cdot}H_2O$: 94 mg, $Pd(NH_3)_4Cl_2$: 69 mg, $Pt(NH_3)_4Cl_2$: 51 mg, $HAuCl_4{\cdot}xH_2O$: 60 mg] were added into the aqueous solution (40 mL) and subsequently stirred for 2 h. After evaporation of water from the solution by placing the container in an oven (100 °C) for 10 h, the samples were finely ground using a mortar and pestle and subsequently calcined at 400 °C for 4 h in the air. The amount of each metal nanoparticle (M_n) loaded on TiO_2 corresponds to 1% by weight.

2.6. Measurements of methanol/water (M/W) and methyl formate/water (MF/W) ratios

To measure the M/W ratio of a mixed vapor of methanol and water being fed into the reactor the vapor was also fed on-line into another GC loaded with Porapak Q column, which can safely separate water from methanol. The calibration curve for water was obtained by directly injecting 1 μL of each solution having 100, 200 and 500 ppm of water, respectively, in methanol. The MF/W ratio was also measured similarly.

2.7. GC analyses

The product stream was introduced on-line into one or two gas chromatographs (GCs) equipped with a flame ionization detector (FID) and a pulsed discharge detector (PDD). Several different types of GC columns were used to quantitatively analyze the products. The types of columns used for the analyses of various products, the oven temperatures, types of detectors, types and flow rates of carrier gases, and the corresponding retention times are listed in Table SI-1-1. The conditions for GC–MS (types of injector and columns, flow rates helium, retention times of the products) by head gas analyses are listed in Table SI-1-2. The corresponding analyses condition by on-line GC–MS is listed in Table SI-1-3.

2.8. Turnover frequency calculation

We took the followings into accounts during the calculation of TOF values. Out of 350 mg of a catalyst, we figured out that less than one third of the catalyst layer receives photons. So we multiplied 1/3 to the weight of catalyst. Because the irradiation area is 6 cm^2, we multiplied 1/6 to the weight of catalyst. Because the weight of M_n in M_n–TiO_2 is 1%, we also multiplied 1/100 to the weight of M_n–TiO_2. Finally, taking the diameter of Pt (for example, 3 nm) into account, we calculated the maximum number of Pt_n particles which receive photons.

2.9. Calibration curves for GC analyses

The calibration curves were obtained for the quantitative analyses of the reactants and products. The standard gas mixtures (CH_4: 1012, CO_2: 499, CO: 505, CH_3OH: 496 and H_2: 999 ppm in Ar balance gas) were purchased from Air Korea. Other standard gas mixtures (CH_3OH: 19.6 ppm in N_2 balance, HCHO: 7 ppm in air balance, $(CH_3)_2O$: 50.2 ppm in Ar balance, and H_2: 1000 and 2000 ppm in Ar balance) were purchased from RIGAS Korea. Formaldehyde, MF, and DMM were calibrated by preparing an aqueous solution of each compound with the concentrations of 100, 200, and 500 ppm, respectively, and injecting 1 μL of each solution into a GC. As an internal standard, methanol was also added into each solution so the concentration of methanol to be matched with that of the compound of interest (100, 200, and 500 ppm, respectively), and the areas of the compound of interest was calibrated with that of methanol. Since formic acid cannot be detected with a GC, the amount of formic acid input was calculated by acid–base titration. Thus, a NaOH solution (5 mL) with a known concentration was prepared in a flask and into this 20 μL of methyl orange solution was added. This flask was placed inside the reactor and the temperature of the reactor was kept at 10 °C to prevent the formic acid vapor escaping from the flask. A small magnetic stirring bar was rotated with the help of a magnetic stirrer. Subsequently,

the moist formic acid vapor was bubbled into the reactor under the same condition the photocatalytic oxidation was carried out. The end point of titration was determined by the sharp change in the color from yellow to orange. The period (time) to reach the equivalence point was carefully observed and this experiment was repeated for three times. From the required period of time the concentration of HCOOH in the vapor stream was calculated.

2.10. Diffuse reflectance UV–vis spectra

Rigorously dried M_n–TiO_2 powders (dried at 200 °C for 5 h under vacuum at 10^{-4} Torr) were prepared and transferred into a glove box charged with dry Ar. Inside the glove box, 0.5 g of a M_n–TiO_2 was loaded into a flat cylindrical fused silica cell (diameter = 19 mm, I.D., thickness = 2 mm, Precision cells Inc. US) and 50 μL of the reagent of interest (methanol, methyl formate, or dimethoxy methane) was introduced into the flat cylindrical cell under the dim red light. The cylindrical cell loaded with TiO_2 and an organic reagent was tightly capped not to allow air goes into the cell. The sample-loaded and tightly-capped cell was wrapped with a piece of black cloth inside the glove box and brought out as such to the atmosphere. The diffuse reflectance spectrum of the sample (kept in the dark) was measured on a UV–vis–NIR spectrometer equipped with an integrating sphere. After obtaining a spectrum, the sample was irradiated with a solar simulated light for a certain period of time, and its diffuse reflectance UV–vis spectrum was taken. The irradiated sample was then exposed to the atmosphere for 10 min and the UV–vis spectrum was taken one more time. In the case of formaldehyde and formic acid, which were obtained in the form of aqueous solutions, 50 μL of each was added into the flat cylindrical fused silica cell, equilibrated in the dark for 30 min, evacuated for 5 min, and charged with Ar. The evacuation/charge with Ar cycle was repeated two more times to remove oxygen from the cell. The rest of the measurements of UV–vis spectra of the samples are the same.

3. Results and discussion

3.1. Characterization of $(MO)_n$

The sizes of $(MO)_n$ loaded on TiO_2 were 2–5 nm $(PdO)_n$, 2–3 nm $(PtO)_n$, 2–10 nm $(AuO)_n$, and 3–5 nm $(CuO)_n$ in Fig. 3. As will be described in detail later in this work, $(AuO)_n$ is in fact Au_n, because $(AuO)_n$ undergoes self-reduction to Au_n during preparation.

3.2. Overview of fifteen reactions that take place during photocatalytic reaction of methanol

The fifteen reactions (denoted as R_n with n = 1–15, Scheme 1) are photocatalytic dehydrogenation of methanol to formaldehyde (R_1), thermal hydration of formaldehyde to methanediol (R_2), photocatalytic dehydrogenation of methanediol to photocatalytic dehydrogenation of methanol to formaldehyde (R_1), thermal hydration of formaldehyde to methanediol (R_2), photocatalytic dehydrogenation of methanediol to formic acid (R_3), thermal esterification of formic acid and methanol to MF (R_4), photocatalytic dehydrogenation of formic acid to CO_2 (R_5), thermocatalytic coupling of formaldehyde and methanol to methoxymethanol (R_6), photocatalytic (R_7) and thermocatalytic (R_8) dehydrogenation of methoxymethanol to MF in the presence of O_2, thermocatalytic coupling of methoxymethanol and methanol to DMM (R_9), photocatalytic hydrolysis of DMM to methanol and formaldehyde (R_{10}), photcatalytic decomposition of dry DMM to dimethyl ether (DME) and formaldehyde (R_{11}), thermocatalytic hydrolysis of MF to formic acid and methanol (R_{12}), and photocatalytic decomposition of dry MF to methanol and CO_2 (heterolysis, R_{13}), to two formaldehyde (homolysis, R_{14}), and to CH_4 and CO_2 (heterolysis, R_{15}).

Among the aforementioned fifteen reactions, R_2 is a known reversible reaction with the equilibrium being favorable to methanediol at room temperature [67]. We found that R_3 is also reversible while the rest of the reactions are irreversible (*vide infra*). Ten reactions (R_1, R_3, R_5, R_7, R_{10}–R_{15}) are purely photocatalytic regardless of the nature of carrier gas. R_2 and R_4 are fast non-catalytic thermal reactions while R_6, and R_9 are slow thermocatalytic reactions regardless of the carrier gas. Interestingly, R_8 is thermocatalytic only in the O_2 environment. Thus, with O_2 as the carrier gas, both R_7 and R_8 undergo simultaneously. The dehydrogenation reactions (R_1, R_3, R_5, R_7, and R_8) are rate-determining, being accelerated (R_1, R_3, R_5, and R_7) or triggered (R_8) by O_2. Among the dehydrogenation reactions, only R_3 (but not R_1, R_5, R_7, and R_8) is suppressed by H_2 due to its reversible nature. With Pd_n–TiO_2 as the photocatalyst, the photocatalytic homolysis of MF to formaldehyde (R_{14}) is also suppressed by H_2 (by ~four times than when Ar is used as the carrier gas), despite the fact that it is not a dehydrogenation reaction (*vide infra*). A future study is necessary to elucidate the reasons.

There are two pathways from methanol to MF, hydrous ($R_2 \rightarrow R_3 \rightarrow R_4$) and anhydrous ($R_6 \rightarrow R_7$ and $R_6 \rightarrow R_8$). The former is faster than the latter by about 4 times. The rate of R_n is denoted as rR_n. The following phenomena were deduced; $rR_5 \ll rR_4$, $rR_9 \ll rR_7$, $rR_9 < rR_8$, $rR_7 < rR_8$ in the O_2 environment, $rR_{11} \ll rR_{10}$, $rR_{10} < rR_1$ by about 3 times, $rR_{12} \gg (rR_{13}$ and $rR_{15})$, $rR_{12} > rR_{14}$, $rR_{14} \gg (rR_{13} \approx rR_{15})$ by about 140 times (*vide infra*). The last phenomenon is highly interesting in the sense that the calculated activation energies for MF thermolysis have been reported to be increasing in the order, $R_{13} < R_{14} < R_{15}$ [68,69]. The elucidation of the reason for this phenomenon is an interesting subject for future studies.

3.3. Photocatalytic reaction of methanol

We found that the methanol-to-water (M/W) ratio sensitively affects the conversion and product distribution. So the reactions are classified into four categories depending on the M/W ratio: M/W = 0.3, 5, 500, and ∞. The conditions of M/W = 0.3 and 5 were obtained by passing a carrier gas (6 mL min^{-1}) through the aqueous solutions of methanol with the concentrations of 1000 and 5000 ppm, respectively, at room temperature. The condition of M/W = 500 was obtained by using a methanol solution having 30 ppm of water. The condition of M/W = ∞ was obtained by using a rigorously dried methanol and rigorously dried reactor and stainless steel tubes.

3.3.1. Under the condition of M/W = 0.3

When M/W = 0.3, with the methanol input of ~2 μmol h^{-1} cm^{-2} and Ar as the carrier gas, only hydrogen and CO_2 were produced (Table 1, entry 1). This reaction thus becomes the unprecedented photocatalytic methanol steam reforming which occurs at room temperature by sun light (Eq. (1)).

$$CH_3OH + H_2O \xrightarrow[(MO)_n-TiO_2]{\text{sun light, Ar}} 3H_2 + CO_2 \quad (1)$$

Considering that the thermal steam reforming is usually carried out at 150–340 °C [70–72], the above photocatalytic steam reforming is highly novel and energy saving.

Upon changing the carrier gas from Ar to CO_2, the conversion rate decreased a bit (from 68 to 53%) (Table 1, entry 2), presumably due to the increase in density of the carrier gas (1.976 g/L at 0 °C, 1 atm) than that of Ar (1.784 g/L at 0 °C, 1 atm), which is likely to cause the decrease of the methanol concentration at the bottom of the reactor where $(MO)_n$–TiO_2 catalysts are placed. Nevertheless,

Table 1
Photocatalytic reaction of methanol on M_n–TiO_2 under various conditions.

No	M–TiO_2 M	Carrier Gas[a]	Input[b]	Reacted[b] (Conv)	Major products				Minor products						Mass Balance	
					H_2 Yield (Y_e/Y_t)[c]	TOF (h^{-1})	$HCOOCH_3$(MF) Yield (S)	TOF (h^{-1})	DMM[d] Yield (S)[g]	HCHO Yield (S)[g]	CO_2 Yield (S)[g]	CH_4 Yield (S)[g]	DME[e] Yield (S)[g]	CO Yield (S)[g]	C%	H%
Methanol/water (M/W = 0.3)																
1	Pd	Ar	1.9	1.3 (68)	3.6 (94)	1870	0.00	0	0.00	0.00	1.27 (100)	0.00	0.00	0.00	98	–
2	Pd	CO_2	2.1	1.1 (53)	3.1 (94)	1628	0.00	0	0.00	0.00	NM[f]	0.00	0.00	0.00	–	94
3	Pd	H_2	1.6	0.8 (52)	NM[f]	NM[f]	0.00	0	0.00	0.00	0.80 (100)	0.00	0.00	0.00	99	–
4	Pd	O_2	2.1	1.4 (71)	0.0	0	0.00	0	0.00	0.00	1.40 (100)	0.00	0.00	0.00	93	–
Methanol/water (M/W = 5)																
5	Pd	Ar	4.0	2.6 (67)	6.4 (90)	3,382	0.02 (1.6)	11	0.00	0.00	2.40 (98.4)	0.00	0.00	0.00	93	100
6	Pd	CO_2	4.3	2.3 (54)	5.6 (82)	2941	0.18 (100)	95	0.00	0.00	NM[f]	0.00	0.00	0.00	–	93
7	Pd	H_2	4.6	2.4 (52)	NM[f]	NM[f]	0.23 (19.0)	121	0.00	0.00	1.92 (81)	0.00	0.00	0.00	99	–
8	Pd	O_2	3.5	2.6 (74)	0.0	0	0.24 (19.0)	126	0.00	0.00	2.10 (81)	0.00	0.00	0.00	100	–
Methanol/water (M/W = 500)																
9	Pd	Ar	126	20.0 (16)	17.8 (92)	9348	9.50 (97.2)	4989	0.03 (0.5)	0.08 (0.40)	0.19 (1.00)	0.12 (0.60)	0.01 (0.10)	0.04 (0.20)	96	93
10	Pd	CO_2	166	20.5 (13)	21.3 (103)	10,504	9.60 (97.0)	5042	0.06 (1.0)	0.15 (1.00)	NM[f]	0.24 (1.00)	0.01	0.00	96	98
11	Pd	H_2	115	12.0 (10)	NM[f]	NM[f]	5.70 (97.5)	2994	0.01 (0.3)	0.01 (0.10)	0.01 (0.10)	0.19 (1.60)	0.02 (0.30)	0.01 (0.10)	96	–
12	Pd	O_2	146	34.0 (23)	0.0	0	17.00 (99.3)	8928	0.02 (0.2)	0.03 (0.07)	0.02 (0.05)	0.01 (0.02)	0.01 (0.06)	0.10 (0.30)	100	–
13	Pd	Ar	293	27.0 (9)	16.8 (72)	8823	10.60 (77.4)	5567	1.90 (20.8)	0.27 (1.00)	0.05 (0.20)	0.05 (0.20)	0.05 (0.30)	0.01 (0.01)	100	89
14	Pd	H_2	218	9.2 (4)	NM[f]	NM[f]	3.10 (66.3)	1628	0.87 (27.9)	0.37 (3.90)	0.02 (0.20)	0.04 (0.40)	0.05 (1.10)	0.01 (0.10)	100	–
15	Pd	O_2	229	33.0 (15)	0.0	0	16.20 (97.4)	8508	0.04 (0.4)	0.01 (0.03)	0.64 (1.90)	0.01 (0.03)	0.03 (0.20)	0.01 (0.03)	100	–
16	Pt	Ar	272	21.0 (8)	14.7 (74)	12,696	9.10 (87.1)	7854	0.47 (6.7)	1.16 (5.60)	0.01 (0.05)	0.04 (0.20)	0.03 (0.30)	0.01 (0.05)	100	89
17	Pt	H_2	272	12.0 (5)	NM[f]	NM[f]	5.50 (90.3)	4750	0.30 (7.4)	0.13 (1.00)	0.01 (0.08)	0.01 (0.08)	0.06 (1.00)	0.01 (0.08)	100	–
18	Pt	O_2	233	33.0 (14)	0.0	0	15.70 (94.4)	13,560	0.06 (0.5)	0.02 (0.06)	1.63 (4.90)	0.01 (0.02)	0.01 (0.10)	0.01 (0.02)	100	–
19	Cu	Ar	253	14.6 (6)	12.7 (90)	4975	7.00 (98.4)	2742	0.04 (0.9)	0.01 (0.07)	0.05 (0.35)	0.01 (0.07)	0.01 (0.10)	0.02 (0.10)	96	92
20	Cu	H_2	275	8.5 (3)	NM[f]	NM[f]	3.60 (97.3)	1410	0.04 (1.6)	0.01 (0.10)	0.01 (0.10)	0.01 (0.10)	0.02 (0.50)	0.01 (0.10)	84	–
21	Cu	O_2	230	26.0 (11)	0.0	0	10.40 (91.5)	4074	0.06 (0.8)	0.03 (0.10)	1.66 (7.30)	0.01 (0.04)	0.01 (0.10)	0.02 (0.10)	87	–
22	Au	Ar	236	9.0 (4)	7.0 (83)	5908	4.10 (90.5)	3460	0.19 (6.3)	0.07 (0.80)	0.08 (0.90)	0.11 (1.20)	0.01 (0.20)	0.01 (0.10)	100	91
23	Au	H_2	236	9.6 (4)	NM[f]	NM[f]	3.90 (80.3)	3293	0.51 (15.8)	0.22 (2.30)	0.01 (0.10)	0.02 (0.20)	0.06 (1.20)	0.01 (0.10)	100	–
24	Au	O_2	261	31.0 (12)	0.0	0	13.80 (98.6)	11,647	0.08 (0.8)	0.03 (0.10)	0.09 (0.30)	0.01 (0.04)	0.01 (0.10)	0.10 (0.04)	90	–
25	none	Ar	229	0.0	0.0	0	0.00	0	0.00	0.00	0.00	0.00	0.00	0.00	–	–
26	none	H_2	131	0.0	NM[f]	NM[f]	0.00	0	0.00	0.00	0.00	0.00	0.00	0.00	–	–
27	none	O_2	131	0.0	0.0	0	0.00	0	0.00	0.00	0.00	0.00	0.00	0.00	–	–
Methanol/water (M/W = ∞)																
28	Pd	Ar	137	4.7 (4)	4.3 (96)	2258	2.10 (89.2)	1103	0.04 (2.5)	0.12 (2.50)	0.12 (2.50)	0.03 (0.70)	0.01 (0.40)	0.10 (2.10)	97	99
29	Pd	CO_2	167	10.7 (6)	10.4 (100)	5478	5.20 (98.0)	2731	0.02 (0.6)	0.06 (0.60)	NM[f]	0.03 (0.30)	0.01 (0.20)	0.00	98	98
30	Pd	H_2	132	4.6 (4)	NM[f]	NM[f]	2.20 (92.2)	1155	0.01 (0.6)	0.01 (0.20)	0.01 (0.20)	0.19 (4.00)	0.06 (2.50)	0.01 (0.30)	95	–
31	Pd	O_2	160	21.0 (13)	0.0	0	9.90 (97.5)	5199	0.02 (0.3)	0.05 (0.20)	0.50 (0.20)	0.06 (0.30)	0.05 (0.50)	0.18 (0.90)	97	–

[a] Flow rate = 6 mL min^{-1}.
[b] In μmol h^{-1} cm^{-2}.
[c] Y_e/Y_t = (experimental yield/theoretical yield) × 100, in %.
[d] DMM = dimethoxy methane.
[e] DME = dimethyl ether.
[f] NM = not measured.
[g] S = Selectivity.

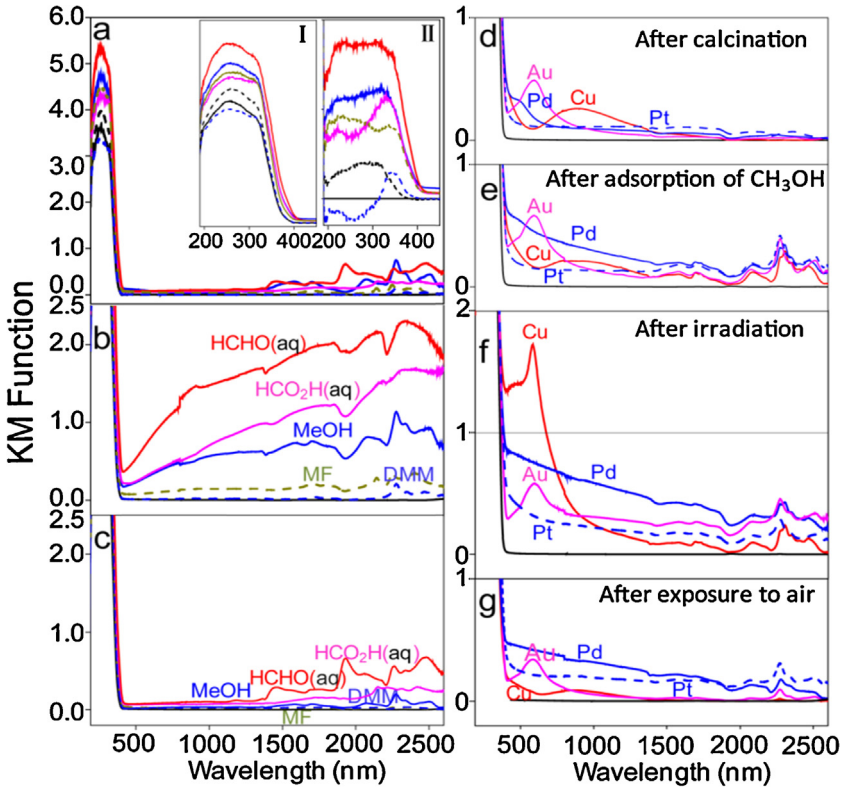

Fig. 1. Diffuse reflectance spectra of the methanol–TiO_2 CT bands, solvated electrons, metal nanoparticles. (a) TiO_2 adsorbed with methanediol or aqueous formaldehyde (red), methanol (blue solid), methyl formate (light green), aqueous formic acid (purple) moisture (back dash), none (black solid), and DMM (blue dash) in the 200–2600 nm range, in the 200–500 nm range (inset I), and the difference spectra with respect to that of dry TiO_2 (inset II) in the 200–500 nm range. (b) TiO_2 adsorbed with methanediol or aqueous formaldehyde (red), methanol (blue solid), methyl formate (light green), and DMM (blue dash) after irradiation with the solar simulated light for 10 min. (c) after exposure to the atmosphere for 5 min. (d), M_n-loaded TiO_2 immediately after calcination. (e) After adsorption of methanol. (f) After irradiation with the solar simulated light for 10 min. (g) after exposure to the atmosphere for 5 min. (For interpretation of the references to color in this figure legend, the reader is referred to the web version of this article.)

the selectivity to H_2 was the same with the case when Ar was used as the carrier gas. Upon switching the carrier gas from Ar to H_2, the conversion rate decreased from 68 to 52%, due to the reversible nature of R_3. In fact the density of H_2 (to 0.08988 g/L at 0 °C, 1 atm) is significantly lower than that of Ar. This is expected to give a positive effect to the conversion rate because the concentration of methanol vapor at the bottom of the reactor will increase upon using a very light gas H_2 as the carrier gas. However, the decrease of the conversion rate caused by reversibility of R_3, under this condition of very small methanol input, is less significant than when the amounts of methanol input are much larger (over 100 μmol h^{-1} cm^{-2}, see Table 1, entries 9–31).

With O_2 as the carrier gas, only CO_2 is formed and no H_2 is detected, indicating that all H_2 is converted to water under the reaction condition. The positive effect of O_2 on the conversion rate is less apparent than when the methanol inputs are larger (over 100 μmol h^{-1} cm^{-2}, see Table 1, entries 9–31).

3.3.2. Under the condition of M/W = 5

With M/W = 5, the methanol input of ~4 μmol h^{-1} cm^{-2}, and Ar as the carrier gas, MF starts appearing (Table 1, entry 2). Again, the use of CO_2 as the carrier gas instead of Ar also led to a reduction of the conversion rate (from 67 to 54%). Interestingly, in this case the selectivity to MF has increased substantially than when Ar was used as the carrier gas. We propose that this happens due to the following two reasons. First, the thermal reaction R_4 is catalyzed by Brönsted acid. This is quite reasonable because esterification is readily catalyzed by acid. Second, CO_2 produces carbonic acid H_2CO_3 in the atmosphere, which acts as the acid source.

With H_2 as the carrier gas, due to the reversibility of R_3, the selectivity to CO_2 decreased by 17% with respect to that with Ar as the carrier gas. As a result, the increase in selectivity to MF takes place via the anhydrous pathway. The change of the carrier gas from Ar to O_2 led to only a slight increase in the conversion rate (from 67% to 74%), not like the cases with higher inputs of methanol (>100 μmol h^{-1} cm^{-2}), due to the low concentration of methanol (~4 μmol h^{-1} cm^{-2}) in the reactor. Although up to 19% selectivity to MF is obtained under the condition of M/W = 5, the photocatalytic steam reforming (Eq. (1)) is still the most prevalent reaction under this reaction condition.

3.3.3. Under the condition of M/W = 500

With M/W = 500, methanol input higher than 100 μmol h^{-1} cm^{-2}, and Ar, CO_2, and H_2, respectively, as the carrier gas, H_2 (>72%) and MF (66.3%) were produced as the major products (Eq. (2)), caused by activation of R_4 and R_6 in Scheme 1 (Table 1). DMM (6–21%) and other compounds (<6%) such as formaldehyde, CO_2, CO, CH_4, and DME were produced as the minor products (Table 1).

$$CH_3OH \xrightarrow[(MO)_n-TiO_2]{\text{Sun}, \ CO_2, \ Ar, \text{or } H_2} H_2 + HCOOCH_3 + \text{minor products} \quad (2)$$

In the cases when M = Pd, Pt, and Cu, the use of H_2 as the carrier gas led to the decrease in conversion rate, due to the suppression of R_3 (compare entries 10 and 11, 13 and 14, 19 and 20, respectively, in Table 1). However, when M = Au, the use of H_2 did not cause the decrease in conversion rate with respect to that of Ar as the carrier gas. In fact, because H_2 is a very light gas (*vide supra*), the

conversion rate is expected to increase because the local concentration near the catalyst is much higher with H_2 as the carrier gas than when other heavier gases as carrier gases. In view of this it can be said that the fact that the same conversion rate was observed with H_2 as the carrier gas already suggests that the conversion rate has decreased substantially. The use of O_2 as the carrier gas led to a marked increase in conversion rate regardless of the nature of M. This shows that O_2 greatly accelerates the dehydrogenation reactions R_1, R_3, R_5, and R_7, and that they are the rate determining steps. Under this condition, because H_2 is converted to H_2O by O_2, MF (91.5–99.3%) remains as the single major product (Eq. (3)). The minor products are DMM, formaldehyde, carbon dioxide, carbon monoxide, methane, and DME.

$$CH_3OH \xrightarrow[(MO)_n-TiO_2]{\text{sun light, } O_2 \text{ moisture}} HCOOCH_3 + \text{minor products} \quad (3)$$

Thus, the above reactions would be useful for photocatalytic conversion of methanol to nearly pure MF. In particular, Pd_n–TiO_2 is very useful for this purpose because both the conversion rate (34 μmol h^{-1} cm^{-2}, 23%) and the selectivity to MF (99.3%) were highest (entry 12, Table 1).

The measured O_2-induced increases in conversion rate (with respect to Ar) were 67, 75, 83, 300% for M = Pd, Pt, Cu, and Au, respectively, for similar methanol inputs (>200 μmol h^{-1} cm^{-2}, compare entries 13/15, 16/18, 19/21, and 22/24, in Table 1). Thus, the conversion rate increased in the order of Pd < Pt < Cu ≪ Au, indicating that the rate of spontaneous dehydrogenation (without the help of O_2) decreases in the opposite order. Indeed, the methanol conversion rate under Ar decreased in the order of Pd (9%) > Pt (8%) > Cu (6%) > Au (4%). The significant decreases in selectivity to DMM (0.2–0.8%) by O_2 show that $(R_2 + R_3) \gg R_6$. The fact that the selectivity to CO_2 is also low (<7.3%), despite the fact that O_2 greatly accelerates the CO_2 formation reaction R_5, indicates that $R_4 \gg R_5$ under a methanol rich condition even in the atmosphere of O_2, in particular with M_n = Pd_n and Au_n because in these cases the selectivities to CO_2 are less than 0.3%. Thus, with O_2 as the carrier gas, the main stream reactions are R_1, R_2, R_3, and R_4.

3.3.4. Under the condition of M/W = ∞

Under this condition and with the methanol input higher than 100 μmol h^{-1} cm^{-2}, and Ar, CO_2, and H_2, respectively, as the carrier gas, H_2 (>96%) and MF (>89%) were produced as the major products (Eq. (2)). However, the overall methanol conversion rate decreased. For example, while the conversion is 16% with M/W = 500 (entry 9 in Table 1), it becomes 4% (entry 28 in Table 1) with M/W = ∞ despite the fact that the carrier gas (Ar) and methanol inputs were similar (∼130 μmol h^{-1} cm^{-2}). Also compare the conversion rate of 13% for M/W = 500 (entry 10 in Table 1) with that of M/W = ∞ (6%) (entry 29 in Table 1) for a similar methanol input of ∼166 μmol h^{-1} cm^{-2} with CO_2 as the carrier gas.

3.3.5. Moisture-induced acceleration of conversion rate

The phenomenon that the conversion rate is significantly lower under the dry condition (M/W = ∞) than under the moist condition (M/W = 500) served as an important reasoning for us to conclude that the hydrous ($R_2 \rightarrow R_3 \rightarrow R_4$) pathway is much faster than the anhydrous ($R_6 \rightarrow R_7$ and $R_6 \rightarrow R_8$) pathway. Because the conversion rate is 4% (entry 28 in Table 1) in the case of M/W = ∞ while that of M/W = 500 is 16% (entry 9 in Table 1), it is also concluded that the hydrous pathway is faster than the anhydrous one by 4 times (*vide supra*). Thus, the methanol conversion rate is much higher in the presence of small amounts of moisture then in the complete absence of moisture.

3.3.6. Order of relative rates

The above reactions with M/W ≥ 500 are very useful for the conversion of methanol to hydrogen and/or MF by properly choosing the carrier gas. As have been noted, the three factors that sensitively affect the methanol conversion rate and the product distribution are the M/W ratio, the nature of carrier gas, and the nature of M_n (Table 1). Thus, it has been deduced that, for H_2 and/or MF formation, the methanol conversion rate increases in the order of (M/W = 500) > (M/W = ∞), in the order of O_2 > Ar ≈ CO_2 > H_2, and in the order of Pd > Pt > Cu > Au. In the case of CO_2 reduction with H_2O in single chamber reactions, the yields for CH_3OH have been observed to be higher with Cu/TiO_2 as the catalyst [20,37,38b,40]. This seems to arise because the reverse reaction, that is the decomposition of methanol, is slower with Cu/TiO_2 as the catalyst.

3.3.7. Reversible and rate-determining R_3

In the case of M/W = 500, the change of the carrier gas from Ar to H_2 leads to a substantial decrease in methanol conversion rate [see Pd_n: 16% → 10% (entries 9 and 11), Pd_n: 9% → 4% (entries 13 and 14), Pt_n: 8% → 5% (entries 16 and 17), Cu_n: 6% → 3% (entries 19 and 20) in Table 1]. Since the hydrous pathway is the major (faster) pathways for the conversion of methanol to H_2 and MF (four times faster than the anhydrous pathway), this phenomenon takes place only when R_3 is reversible (rR_3 decreases as the concentration of H_2 increases). Another evidence for the reversibility of *R3* (in the case of M/W = 500) is the increases in the produced amounts of DMM and DME (the minor products that appear only from the anhydrous pathway) upon changing the carrier gas from Ar to H_2. For DMM, the increases were Pd_n: 20.8% → 27.9%, Pt_n: 6.7% → 7.4%, Cu_n: 0.9% → 1.6%, and Au_n: 6.3% → 15.8%. For DME, the increases were Pd_n: 0.3% → 1.1%, Pt_n: 0.3% → 1.0%, Cu_n: 0.1% → 0.5%, and Au_n: 0.2% → 1.2%. Therefore, in the case of Au_n, although the conversion rate remained constant (4%) even after changing the carrier gas from Ar to H_2 (compare entries 22 and 23 in Table 1), the increases in the produced amounts of DMM and DME indicate that R_3 is also reversible when M_n = Au_n. The fact that R_3 affects the overall conversion rate indicates that this reaction is also the rate determining reaction for the formation of H_2/CO_2 and H_2/MF.

In the case of M/W = ∞, the methanol conversion rate does not decrease as the carrier gas is changed from Ar to H_2, because in such a highly dry condition the hydrous pathway, including R_3, does not operate. Even under this rigorously dry condition, H_2 (96%) and MF (89–92%) is still the major products indicating that the anhydrous pathway is operating. Knowing this, the facts that the carrier gas change from Ar to H_2 does not decrease the conversion rate and the product selectivities remain essentially the same indicate that R_7 is not affected by the presence of a large amount of H_2. This shows that R_7 is not a reversible reaction.

3.3.8. Dark reactions

In the dark, essentially no products were produced (Table SI-2). Coupled with the results obtained in the absence of $(MO)_n$ on TiO_2 (Table 1, entries 25–27), the results of the dark reactions indicate that the overall reaction of methanol oxidation with and without moisture on $(MO)_n$–TiO_2 is photocatalytic.

3.3.9. Effect of moisture, carrier gas, concentration, and nature of M_n on selectivities of minor products

Under the completely anhydrous condition (M/W = ∞) the faster hydrous pathway ($R_2 \rightarrow R_3 \rightarrow R_4$) to MF becomes completely blocked regardless of the use of H_2 as the carrier gas or not. This gives a higher probability to R_6, which subsequently gives higher opportunities to R_9, R_{11}, R_{13}, R_{14}, and R_{15}. By this way, the relative selectivities to the minor products [in particular to CH_4 (4%) arising from R_{15} and DME (2.5%) arising from R_{13}] increase significantly (Table 1, entry 30). Recall that among the three unimolecular

decomposition reactions of dry MF (R_{13}, R_{14}, and R_{15}), homolysis to dry formaldehyde is fastest (faster than the others by ~140 times).

Under the slightly moist condition (M/W = 500), the use of H_2 as the carrier gas suppresses only the hydrous pathway (R_3) but not the rest of the reaction paths. Under this moist condition (M/W = 500), the hydrolysis rate of MF (rR_{12}), which is much faster than rR_{13}, rR_{15}, and even rR_{14} [recall that $rR_{12} \gg (rR_{13}$ and $rR_{15})$ and $rR_{12} > rR_{14}$], is still active. As a result, while the selectivity to DMM increases (compare entries 13 and 14, going from 20.8% with Ar to 27.9% with H_2, entries 19 and 20, going from 0.9 with Ar to 1.6 with H_2, and entries 22 and 23, going from 6.3 with Ar to 15.8 with H_2 in Table 1), the relative selectivities to minor products arising from R_{13} and R_{15} (CO and CH_4) become suppressed.

3.3.10. Necessity of M_n for photoconversion

The presence of M_n on TiO_2 is essential for the above photocatalytic reactions because no products were formed with bare TiO_2 as the catalyst (Table 1, entries 25–27), regardless of the carrier gas.

3.3.11. Turnover frequency for H_2 and MF production

The highest turnover frequencies for H_2 and MF formation per h (TOF) per a 3-nm M_n particle were 12,696 and 7,854 h^{-1}, respectively, under the condition of M/W = 500, $M_n = Pt_n$, and the carrier gas = Ar (Table 1, entry 16). With O_2 as the carrier gas, the highest TOF for MF formation was 13,560 h^{-1} under the condition of M/W = 500 and $M_n = Pt_n$ (Table 1, entry 18). Although there are reports that the irradiation of the methanol adsorbed on bare TiO_2 with 400 nm or UV light produces formaldehyde or formaldehyde and MF [73,74], we did not observe any products under our experimental condition when bare TiO_2 was used as the catalyst (Table 1, entries 25–27). In the dark, even with $(MO)_n$–TiO_2 as catalysts, essentially no products were produced confirming that the overall reaction is photocatalytic (SI-2).

3.4. Photocatalytic reaction of formaldehdye

To study the reaction with formaldehyde as the reactant, an aqueous formaldehyde solution consisting of water (47–52%), formaldehyde (37%), and methanol (10–15%) was used as the reactant because of the difficulty to obtain pure anhydrous formaldehyde, not being stabilized with methanol. Although the formaldehyde-to-methanol (F/M) ratio is not so high in the solution (2.5–3.7), it greatly increased to ~20 when the carrier gas was passed through this solution at room temperature because the boiling point of formaldehyde (−19 °C) is much lower than that of methanol (64.7 °C).

3.4.1. Under the condition of F/M = 20

With this stream as the reactant and $(PdO)_n$–TiO_2 and Ar as the representative catalyst and carrier gas, respectively, the observed conversion rate was only 7% with respect to the input amount of formaldehyde despite the fact that the input amount is not so high (33 μmol h^{-1} cm^{-2}). Although the conversion rate was low, H_2 (92%) and CO_2 (96%) were produced in the ratio of ~2:1 (Eq. (4)) and a small amount of MF (4%) was also produced (Table 2).

$$HCHO + H_2O \xrightarrow[(PdO)_n-TiO_2]{\text{sun light,Ar}} 2H_2 + CO_2 \quad (4)$$

Based on the reaction flow in Scheme 1, production of one equivalent of CO_2 accompanies production of two equivalents of H_2 from formaldehyde and three equivalents of H_2 from methanol. Therefore, based on the reacted amounts of formaldehyde (2.4 μmol) and methanol (1.35 μmol), the theoretical amount (Y_t) of H_2 is 8.85 μmol. When taking the fact that some hydrogen atoms reside in MF (0.08 μmol which is equivalent to 0.16 μmol of H_2) into account the actual Y_t is 8.77 μmol. Because the experimentally observed amount (Y_e) is 8.07 μmol, the yield [$(Y_e/Y_t) \times 100$, in %] is 92%. This result proves the existence of the $R_2 + R_3 + R_5$ pathway. Under the condition where the concentration of methanol is low, R_5 takes place readily because R_4 is suppressed effectively.

With H_2 as the carrier gas, the formaldehyde conversion rate and the carbon dioxide yield significantly decreased due to the reversibility of R_3 (Table 2). Instead, the selectivity to MF increased sharply (from 4 to 47%), due to the activation of the anhydrous pathway to MF. In contrast, with O_2 as the carrier gas, carbon dioxide and water are produced as the major products (Eq. (5)), and the conversion rate increased by 28.5% than with Ar as the carrier gas (Table 2). The significant decrease in selectivity to MF upon changing the carrier gas from H_2 to O_2 (47 to 3%) indicates that R_3 and R_5 become highly activated, which pulls the reaction toward the formation of carbon dioxide (Eq. (5)). This phenomenon can be effectively utilized for the removal of formaldehyde from the contaminated air [54,75,76].

$$HCHO + O_2 \xrightarrow[(PdO)_n-TiO_2]{\text{sun}} CO_2 + H_2O \quad (5)$$

3.4.2. Under the condition of F/M = 0.3

With decreasing the F/M ratio to 0.3 and Ar as the carrier gas, in other words with increasing the relative concentration of methanol, H_2 (~73%) and MF (69%) became the major products and the selectivity to DMM (31%) increased (Table 2). However, carbon dioxide was not produced. The increase in MF yield seems to arise from the activation of both R_4 and R_6. However, the large increase in DMM accompanying no carbon dioxide formation indicates that the formation of MF occurs via R_6. Furthermore, the observation that the selectivity to DMM is smaller than that of MF indicates that $rR_7 > rR_9$.

With H_2 as the carrier gas, the selectivities to MF (69%) and DMM (31%) remain the same (Table 2). With O_2 as the carrier gas, the conversion rate increased to 10.3%. Simultaneously, the selectivity to MF increased sharply (91%) while that to DMM decreased significantly (9%) (Table 2). This phenomenon indicates that R_7 and R_8 become activated by O_2.

3.4.3. Thermocatalytic reactions of formaldehdye and methanol

In the dark, with Pd_n–TiO_2 as the catalyst, essentially no reaction takes place under the condition of F/M = 20, regardless of the nature of carrier gas (Table SI-3). However, when the methanol input was increased so that F/M = 0.3 and with Ar or H_2 as the carrier gas, DMM is produced as the major product (84–91%, Eq (6)) through R_6 and R_9, which are thermocatalytic pathways, and due to inactivation of R_3, R_7, R_{10}, and R_{11}, which are photocatalytic pathways (Table 2).

$$CH_3OH + HCHO \xrightarrow[(PdO)_{n-}]{\text{sun light,Ar or } H_2} (CH_3O)_2CH_2 \quad (6)$$

In the dark with O_2 as the carrier gas, MF became the major product (86%) and the yield of DMM decreased to 14%, due to the presence of the anhydrous thermocatalytic pathway to MF (R_8) which opens in the presence of O_2, and the phenomenon that $rR_8 > rR_9$. Interestingly, while the yield of MF from the thermocatalytic pathway with O_2 as the carrier gas was 9.9 μmol h^{-1} cm^{-2} that from the photoreaction was 16.0 μmol h^{-1} cm^{-2}. Because MF is formed by both photocatalytic (R_7) and thermocatalytic (R_8) pathways with O_2 is the carrier gas, the pure yield arising from photocatalytic (R_7) pathway should be 6.1 μmol h^{-1} cm^{-2}. This result shows the important phenomenon that the thermocatalytic process in the presence of O_2 (R_8) is faster than the photocatalytic process in the presence of O_2 (R_7) with the ratio of 9.9:6.1 or 1.6:1. Thus, $rR_8 = 1.6rR_7$ under the O_2 environment.

Table 2
Photocatalytic reaction of formaldehyde on $(PdO)_n$–TiO_2 under various conditions.

No.	Reactant	Carrier gas[a]	Input[b] (F/M)[c]	Reacted[b] (Conv)	H_2 (Y_e/Y_t)[d]	CO_2 (S)[e]	$HCOOCH_3$ (S)[e]	DMM (S)[e]	Mass balance C%	H%
Formaldehyde/methanol (F/M) = ~20, formaldehyde/water (F/W) = ~1.4, catalyst										
1	HCHO/CH_3OH	Ar	33/2.1	2.4/1.3 (7.0/64.0)	8.05 (91)	3.48 (96.0)	0.08 (4.0)	0.0	97	93
2	HCHO/CH_3OH	H_2	44/1.6	1.9/0.5 (4.0/32.0)	NM[f]	1.10 (53.0)	0.48 (47.0)	0.0	85	–
3	HCHO/CH_3OH	O_2	44/1.5	3.8/1.2 (9.0/77.0)	0.00	4.40 (97.0)	0.07 (3.0)	0.0	91	–
Formaldehyde/methanol (F/M) = ~0.3, formaldehyde/water (F/W) = ~1.4, catalyst										
4	HCHO/CH_3OH	Ar	24/75	3.2/15.7 (14.0/21.0)	6.70 (~73)	0.00	6.10 (69.0)	1.8 (31.0)	93	–
5	HCHO/CH_3OH	H_2	34/85	8.1/16.6 (24.0/20.0)	NM[f]	0.00	8.30 (69.0)	2.5 (31.0)	98	–
6	HCHO/CH_3OH	O_2	32/75	10.3/25.1 (33.0/33.0)	0.0	0.10 (0.3)	16.00 (91.1)	1.0 (8.6)	99	–
Formaldehyde/methanol (F/M) = ~0.3, formaldehyde/water (F/W) = ~ 1.4, no catalyst										
7	HCHO/CH_3OH	Ar	24/75	0.8/1.6 (3.3/2.1)	0.33 (nc[g])	0.00	0.22 (20.0)	0.6 (80.0)	–	–
8	HCHO/CH_3OH	H_2	34/85	0.9/1.9 (2.6/2.2)	NM[f]	0.00	0.35 (28.0)	0.6 (72.0)	–	–
9	HCHO/CH_3OH.	O_2	34/61	0.9/1.9 (2.6/3.1)	0.00	0.00	0.35 (28.0)	0.6 (72.0)	–	–

[a] Flow rate = 6 mL min^{-1}.
[b] In μmol h^{-1} cm^{-2}.
[c] Formaldehyde-to-methanol ratio.
[d] Y_e/Y_t = (experimental yield/theoretical yield) × 100, in %.
[e] S = selectivity.
[f] NM = not measured.
[g] nc = not calculated.

3.4.4. Non-catalytic thermal reactions of formaldehyde and methanol

Even in the dark and without any catalyst (Pd_n–TiO_2), formation of MF and DMM in small amounts was observed, regardless of the nature of the carrier gas (Table SI-3). This indicates that there also exist slower noncatalytic thermal pathways from formaldehyde and methanol to methoxymethanol, from methoxymethanol to DMM, and from methoxymethanol to MF at room temperature. Because these pathways are minor they are not indicated in Scheme 1.

3.5. Photocatalytic reaction of formic acid

When a stream of Ar containing the formic acid vapor (27.6 μmol cm^{-1}) and moisture (amount not measured) was fed into the reactor charged with $(PdO)_n$–TiO_2 under the irradiation condition some of the formic acid (9.2 μmol cm^{-1}) produced H_2 (8.9 μmol cm^{-1}) and CO_2 (9.2 μmol cm^{-1}) in almost 1:1 ratio (Table 3) (Eq. (7)).

$$HCO_2H \xrightarrow[(PdO)_n-TiO_2]{\text{sun light,Ar or } H_2} H_2 + CO_2 \quad (7)$$

Eq. (7) is the unprecedented photocatalytic generation of H_2 from formic acid [77]. Even with H_2 as the carrier gas, the reacted amount of formic acid was similar and almost all the reacted formic acid converted to CO_2. This result indicates that the photocatalytic decomposition formic acid (R_5) is irreversible. With O_2 as the carrier gas, the reacted amount of formic acid increased by about two times (19.9 μmol cm^{-1}), indicating that O_2 also accelerates this reaction. In this case, however, the valuable H_2 source from formic acid becomes wasted. In the dark, the conversion becomes very small regardless of the type of carrier gas, indicating that this reaction is not thermocatalytic.

Recently, various thermocatalysts have been developed for decomposition of formic acid to H_2 and CO_2. In this case, temperature swing is the only way to turn on and off the reaction. However, temperature swing lacks the ability to rapidly control the H_2 pressure in the gas storage container, in particular when the volume of the reactor is large. In this respect, the photocatalytic version has a big advantage due to its ability to quickly switch on and off the reaction.

The irreversibility of R_5 is highly valuable because the photocatalytic reaction cannot be inhibited by the preexisting H_2 in the reactor. The measured TOF for R_5 was 4,664 h^{-1} under our gas phase reaction condition, which is much higher than the recently reported values (80–382 h^{-1}) obtained from heterogeneous thermocatalysts [78,79].

The measured TOF for R_5 was 4,664 h^{-1} under our gas phase reaction condition, which is much higher than the recently reported values (80–382 h^{-1}) obtained from heterogeneous thermocatalysts [78,79] and even than the one obtained from the best homogeneous thermocatalyst (647 h^{-1}) [80]. More interestingly, when our reaction was carried out in the liquid phase, the TOF increased to 14,950 h^{-1}. Most importantly, the catalyst does not undergo deactivation and does not produce carbon monoxide even after a continuous usage for a week, unlike heterogeneous thermocatalysts [77,78].

3.6. Photocatalytic hydrolysis of DMM

During the photocatalytic reaction of methanol, due to the phenomenon of $rR_{10} < rR_1$, DMM could be produced as the major minor product. When an Ar stream of moist DMM was fed into the reactor charged with $(PdO)_n$–TiO_2, the major hydrolysis products were methanol and formaldehyde (Eq. (8)).

$$(CH_3O)_2CH_2 + H_2O \xrightarrow[(PdO)_n-TiO_2]{\text{sun light, Ar}} 2CH_3OH + HCHO \quad (8)$$

However, due to the facile hydrous pathway to hydrogen and MF, the final products are H_2, MF, methanol, and formaldehyde, with the selectivities of 90, 80, 10, and 7%, respectively.

3.6.1. Cyclic pseudo reversible reaction

As noted, R_1, R_6, R_9, and R_{10} form a cyclic pseudo reversible reaction. Due to this phenomenon, the nature of carrier gas sensitively affects the rate of DMM conversion. Thus, with H_2 as the carrier gas, the apparent conversion of DMM decreases significantly. With

Table 3
Photocatalytic and thermocatalytic reactions of formic acid on $(PdO)_n$–TiO_2 under different conditions.

No.	Reactant	Carrier gas[a]	Input[b]	Reacted[b] (Conv)	H_2 (Y_e/Y_t)[c]	TOF (h^{-1})	CO_2 (S)[d]	Mass balance C%	H%
Formic acid/water (FA/W) = 6.6, catalyst, light									
1	HCO_2H/H_2O	Ar	27.61	≥9.16 (≥35.0)	8.88 (97)	4664	9.16 (100)	100	97
2	HCO_2H/H_2O	H_2	27.61	≥8.95 (≥32.0)	NM[e]		8.72 (97)	100	–
3	HCO_2H/H_2O	O_2	27.61	≥19.90 (≥72.0)	0.00		19.90 (100)	100	–
Formic acid/water (FA/W) = 6.6, catalyst, dark									
4	HCO_2H/H_2O	Ar	27.61	0.77 (≥2.8)	0.14	74	0.77 (100)	100	–
5	HCO_2H/H_2O	H_2	27.61	0.91 (≥2.8)	NM[e]		0.91 (100)	100	–
6	HCO_2H/H_2O	O_2	27.61	1.02 (≥3.7)	0.00		1.02 (100)	100	–

[a] Flow rate = 6 mL min^{-1}.
[b] In μmol h^{-1} cm^{-2}.
[c] Y_e/Y_t = (experimental yield/theoretical yield) × 100, in %.
[d] S = selectivity in %.
[e] nm = not measured.

dry DMM vapor as the reactant with Ar as the carrier gas, the selectivity to DME increased sharply (to 31%) with respect to that with moist DMM as the reactant with Ar as the carrier gas (3%) (Compare entries 1 and 5, Table 4), confirming the presence of dry decomposition pathway to DME and formaldehyde (R_{11}). The substantial decrease of the conversion rate (from 6 to 1 μmol h^{-1} cm^{-2}) shows that the rate of the photocatalytic hydrolysis of DMM (rR_{10}) is much faster than the dry photocatalytic heterolysis (rR_{11}), that is, $rR_{10} \gg rR_{11}$.

In fact, the ratio of DME and formaldehyde should be 1:1 in R_{11}. However, the appearance of methanol and MF with rather high selectivity to MF indicates that there were still small amounts of moisture in the catalyst and the reactor, and due to the moisture, the unwanted photoctalytic hydrolysis (R_{10}) also undergoes during this experiment. In fact the thermal decomposition of DMM undergoes only in the presence of strong acid such as HZSM-5 zeolite [81]. The reason that the conversion of dry DMM is so low is because Pd_n–TiO_2 provides the basic environment but not the Brönsted acidic environment. Anyway the observation of DME from the catalytic decomposition of dry DMM confirms the existence of R_{11}. The facts that very small amounts of conversion rate were observed when the reactions were carried out in the absence of the catalyst (Pd_n–TiO_2) regardless of the presence or absence of moisture (entries 4 and 6, Table 4) and the observation of very poor conversion rates from the reactions carried out in the dark even in the presence of the catalyst (Table SI-4) confirm that both the hydrolysis and decomposition in the dry state are photocatalytic reactions.

3.7. Thermocatalytic hydrolysis and unimolecular decomposition of MF

The purchased MF contains small amounts of methanol. So, MF vapor inevitably accompanies a small amount of methanol vapor. When MF was fed into the reactor charged with Pd_n–TiO_2 with Ar as the carrier gas, the conversion rate and the product distribution sensitively varied with the MF-to-water (MF/W) ratio. Thus when there is a sufficient supply of moisture, that is, when MF/W = 1.3, with Ar as the carrier gas and Pd_n–TiO_2 as the representative catalyst, only catalytic hydrolysis to methanol and formic acid (R_{12}, Eq. (9)) took place (Table SI-5). This hydrolysis reaction is thermocatalytic because this reaction undergoes readily even in the dark and the irradiation does not increase the conversion (compare Table 5 and Table SI-5). The formation of formic acid is judged by the formation of hydrogen and carbon dioxide, which are produced from formic acid (R_5) in the absence of large amounts of methanol. The reason that the amount of methanol is smaller than that of CO_2 is because methanol is also converted to CO_2 and H_2 under the moisture-rich condition according to Eq. (1). The fact

Table 4
Photocatalytic reaction of DMM on $(PdO)_n$–TiO_2 under different conditions.

No.	Reactant	Carrier gas[a]	Input[b]	Reacted[b] (Conv)	CH_3OH (S)[c]	HCHO (S)[c]	H_2 (S)[c]	$HCOOCH_3$ (S)[c]	CO_2 (S)[c]	CO (S)[c]	[e]DME (S)[c]	CH_4 (S)[c]	Mass balance C%	H%
DMM, moisture, catalyst, DMM/water = ~ 8.3														
1	DMM/H_2O	Ar	236	6.0 (2.5)	1.50 (10)	1.10 (7)	6.4	6.0 (80)	0.0	0.0	0.20 (3)	0.0	83	92
2	DMM/H_2O	H_2	201	3.6 (2.0)	1.80 (17)	0.40 (4)	NM[d]	3.4 (65)	0.0	0.0	0.70 (13)	0.0	96	–
3	DMM/H_2O	O_2	243	11.4 (5.0)	0.95 (3)	0.70 (3)	NM[d]	13.2 (93)	0.0	0.0	0.10 (1)	0.0	83	–
DMM, moisture, no catalyst, DMM/water = ~ 6.4														
4	DMM/H_2O	Ar	182	Trace	0.30 (43)	0.30 (43)	0.0	0.0	0.0	0.0	0.05 (14)	0.0	–	–
DMM, no water, catalyst														
5.	DMM[e]	Ar	196	1.0 (0.6)	0.10 (4)	0.20 (7)	1.1	0.8 (58)	0.0	0.0	0.42 (31)	0.0	82	91
DMM, no water, no catalyst														
6.	DMM[e]	Ar	191	Trace	0.03 (21)	0.05 (36)	0.0	0.0	0.0	0.0	0.03 (43)	0.0	–	–

[a] Flow rate = 6 mL min^{-1},
[b] In μmol h^{-1} cm^{-2},
[c] S = Selectivity in %.
[d] DME = dimethyl ether.
[e] NM = not measured.

Table 5
Photocatalytic reaction of methyl formate (MF) on $(PdO)_n$–TiO_2 under different conditions.

No.	Reactant	Carrier gas[a]	Input[b]	Reacted[b] (Conv)	H_2	HCHO	DMM[d]	CH_3OH	CO	CO_2	CH_4	Mass balance C%	H%
Methyl formate/water/methanol, (MF/H_2O = 0.8–1.4), catalyst													
1	$HCO_2CH_3/H_2O/CH_3OH$	Ar	23.5/0.9/1.23	3.24/–/– (14.0/–)	5.65 (nc[e])	0.00	0.00	2.20	0.00	4.77	0.19	88	84
2	$HCO_2CH_3/H_2O/CH_3OH$	H_2	21.5/0.8/2.95	2.70/–/– (13.0/–)	NM[c]	0.00	0.00	3.98	0.03	3.95	0.03	93	–
3	$HCO_2CH_3/H_2O/CH_3OH$	O_2	39.6/1.4/4.20	6.70/–/– (17.0/–)	0.00	0.00	0.00	5.95	0.02	6.04	0.08	91	–
Methyl formate/water/methanol, (MF/H_2O = 14–20), catalyst													
4	$HCO_2CH_3/H_2O/CH_3OH$	Ar	641.0/20.0/10.00	41.00/–/– (6.0/–)	23.70(nc[e])	43.00	1.46	9.6	0.40	15.6	0.05	91	91
5	$HCO_2CH_3/H_2O/CH_3OH$	H_2	501.0/16.0/14.80	19.00/–/– (4.0/–)	NM[c]	10.70	0.95	15.0	0.23	5.9	0.00	91	–
6	$HCO_2CH_3/H_2O/CH_3OH$	O_2	437.0/14.0/15.60	20.00/–/– (4.5/–)	0.00	10.70	1.49	15.0	0.11	5.9	0.00	90	–
Methyl formate/no water/methanol, (MF/H_2O = ∞), catalyst													
7	HCO_2CH_3/CH_3OH	Ar	834.0/0.0/2.80	22.00/–/1.92 (3.0/–)	0.77 (nc[e])	34.00	0.00	0.88	0.12	1.90	0.13	83	81
8	HCO_2CH_3/CH_3OH	H_2	851.0/0.0/3.16	6.20/–/0.06 (0.7/–)	NM[c]	9.90	0.00	3.01	0.16	2.34	0.00	100	–
9	HCO_2CH_3/CH_3OH	O_2	676.0/0.0/1.15	20.00/–/1.71 (3.0/–)	0.00	33.60	0.00	2.86	0.18	4.29	0.08	95	–
Methyl formate/no water/methanol, (MF/H_2O = ∞), no catalyst													
10	HCO_2CH_3/CH_3OH no cat.	Ar	676.0/0.0/1.23	0.00/–/0.00	NM[c]	0.00	0.00	0.00	0.00	0.00	0.00	0	0

[a] Flow rate = 6 mL min^{-1}.
[b] In μmol h^{-1} cm^{-2}.
[c] NM = not measured.
[d] DMM = dimethoxy methane.
[e] nc = Not calculated.

that the amount of H_2 (5.65 μmol h^{-1} cm^{-2}) is higher than that of CO_2 (4.77 μmol h^{-1} cm^{-2}) also supports the above reasoning.

$$HCO_2CH_3 \xrightarrow[(PdO)_n-TiO_2]{\text{sun light,moisture}} CH_3OH + HCO_2H \quad (9)$$

With H_2 as the carrier gas, the conversion remained nearly the same. With O_2 as the carrier gas, the conversion rate increased slightly. This phenomenon seems to be related to the acceleration of R_1, R_3, and R_5 by O_2.

With a lesser amount of moisture, that is, with MF/W = 20, a significant increase in selectivity to formaldehyde occurred (Table 5) due to the activation of R_{14}, the homolysis of MF to formaldehyde. The simultaneous appearance of carbon monoxide indicates that R_{13} also takes place to a certain extent. With H_2 and O_2, respectively, as the carrier gas the selectivity to formaldehyde decreased substantially while that to methanol increased significantly. This result indicates that, for some reasons we do not understand at this stage, the dry homolysis to formaldehyde (R_{14}) is suppressed by H_2 and O_2. The suppression of R_{14} by H_2 may occur most likely due to the strong adsorption of H_2 onto Pd_n, which gives rise to deactivation of the photocatalytic homolysis of MF. This phenomenon requires a future theoretical investigation.

Under a rigorously dry condition, that is, with MF/W = ∞, with Ar as the carrier gas, the hydrolysis (R_{12}) was suppressed substantially while the homolysis to formaldehyde (R_{14}) became the major reaction (Table 5). The two heterolysis reactions (R_{13} and R_{15}) also took place, albeit small. Notably, the selectivity to formaldehyde is ~280 times larger than those to other heterolysis products, CO and CH_4, indicating that $rR_{14} \gg (rR_{13} \approx rR_{15})$ by ~140 times (Eq. (10)). In fact, it is difficult to obtain dry formaldehyde [82,83]. Accordingly, Eq. (10) would be a very useful reaction. Again as was the case when MF/W = 20, R_{14} is suppressed significantly with H_2 as the carrier gas under the condition of MF/W = ∞. With O_2 as the carrier gas, the conversion rate and the product distribution are similar to those with Ar as the carrier gas.

$$HCO_2CH_3(dry) \xrightarrow[(PdO)_n-TiO_2]{\text{sun light,Ar}} 2HCHO \quad (10)$$

4. Charge-transfer (CT) interaction between reactants and TiO_2

Upon adsorption of methanol onto bare TiO_2, a new absorption band appeared in the 200–400 nm region with the absorption maximum at 320 nm (Fig. 1a). This band is assigned as the methanol-to-TiO_2 CT band. This is reasonable because it is well known that OH-group bearing compounds form ligand-to-metal CT complexes with the TiO_2 surface [84–86] and even aromatic compounds form CT complexes with dry TiO_2 [87]. Likewise, the new absorption bands arising from methanediol (the equilibrium product of formaldehyde), and formic acid adsorbed on TiO_2 are assigned as the corresponding CT bands. By the same analogy, methoxymethanol (the intermediate from R_6) is expected to form a stronger CT complex with TiO_2 than methanol. MF and DMM form weak CT complexes with TiO_2, because they do not have hydroxyl groups. Another reason would be the hydrophobic nature of MF and DMM due to the lack of OH groups.

The TiO_2 powder adsorbed with methanol, methanediol (formaldehyde), and formic acid, respectively, turns bluish gray upon irradiation with the solar simulated light due to the formation of solvated electrons, which disappear instantaneously upon exposure to the atmosphere. The solvated electrons show a broad featureless band in the 400–2600 nm region (Fig. 1b), which disappear immediately upon exposure to the atmosphere (Fig. 1c). Although MF and DMM form weak CT complexes with TiO_2, they readily generate solvated electrons upon irradiation on moist TiO_2 due to the facile hydrolysis reactions that take place, producing methanol, formaldehyde, and formic acid (Fig. 4).

The bare and methanol-adsorbed $(CuO)_n$–TiO_2 show a broad $(CuO)_n$ absorption band at 878 nm (Fig. 1, d and e). Upon irradiation of the latter, the $(CuO)_n$ band disappears and a sharp new absorption band appears at 578 nm due to the surface plasmon absorption of Cu_n (Fig. 1f). This band instantaneously disappears upon exposure to the atmosphere (Fig. 1g), while restoring the $(CuO)_n$ band. In the case $(PtO)_n$–TiO_2, the UV–vis spectra cannot distinguish Pt_n and $(PtO)_n$. Instead, we confirmed the generation of Pt_n by observing the phenomenon that the irradiated powder becomes extremely

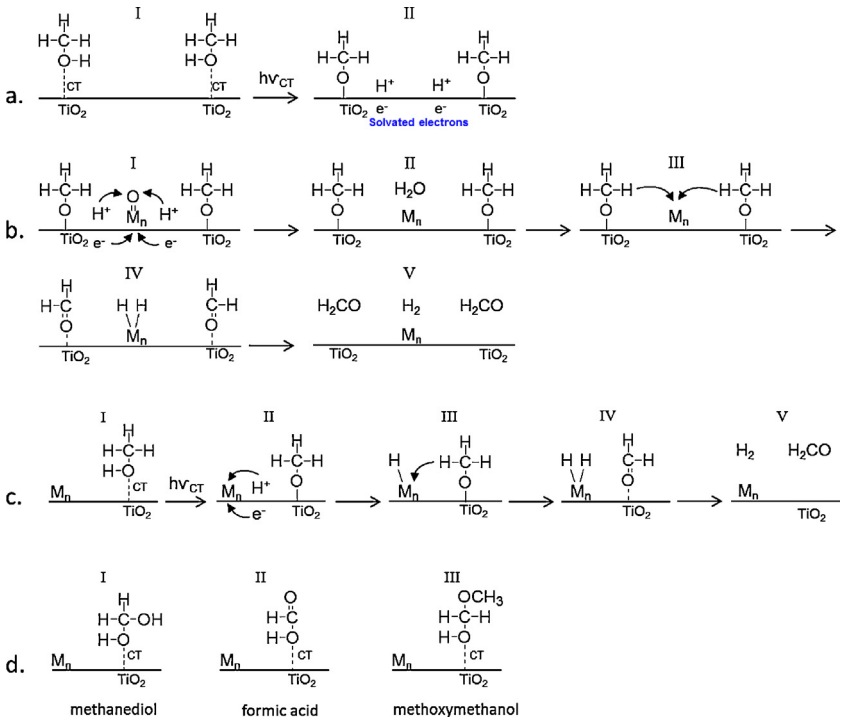

Fig. 2. Proposed mechanism of the photocatalytic dehydrogenation of methanol, methanediol, formic acid, and methoxymethnaol. (a) CT interaction between methanol and TiO_2 and the subsequent photoinduced electron transfer from methanol to TiO_2, giving rise to the production of adsorbed protons and solvated electrons. (b) Formation of TiO_2-adsorbed methoxy groups and the reduction of metal oxide nanoparticles $(MO)_n$ to metal nanoparticles M_n, and the subsequent abstraction of hydrogen atoms from the methoxy groups which leads to the production of formaldehyde and hydrogen. (c) CT interaction between the M_n-loaded TiO_2 and methanol, photoinduced electron transfer from methanol to M_n-loaded TiO_2, formation of hydrido M_n, dehydrogenation from methoxy group, the formation of formaldehyde and hydrogen, and the subsequent desorption of formaldehyde and hydrogen. (d) CT interactions between TiO_2 and methanediol, formic acid, and methoxy methanol, respectively.

pyrophoric, which is a characteristic feature of Pt_n. The methanol adsorbed $(PdO)_n$–TiO_2 also gives Pd_n upon irradiation. In the case of $(AuO)_n$–TiO_2, the surface plasmon band of Au_n appears at 590 nm even before adsorption of methanol, indicating that photoirradiation is not necessary to generate Au_n and that $(AuO)_n$–TiO_2 which we have thought that we have prepared is in fact Au_n–TiO_2.

5. Proposed mechanism

We propose the key mechanism as follows. Methanol forms CT complexes with the TiO_2 surface (Fig. 2a, I). The photoexcitation of the CT band leads to electron transfer from methanol to TiO_2, giving rise to the generation of TiO_2-adsorbed protons and TiO_2-bound methoxy groups (Fig. 2a, II). The transferred electrons exist as solvated electrons in TiO_2 (Fig. 2a, II), which quickly react with oxygen when exposed to the atmosphere. In the Ar or H_2 atmosphere, the solvated electrons and the protons migrate to $(MO)_n$ (Fig. 2b, I), producing M_n and water (Fig. 2b, II). The produced M_n abstracts hydrogen atoms from the TiO_2-bound methoxy groups (Fig. 2b, III), generating the TiO_2-adsorbed formaldehyde and the M_n-adsorbed hydrogen (Fig. 2b, IV). They subsequently desorb into free formaldehyde and hydrogen, regenerating the fresh M_n on TiO_2 (Fig. 3b, V). In the case of $(AuO)_n$–TiO_2, the steps in Fig. 2b are not necessary because Au_n already exists during the sample preparation.

The CT complexation (Fig. 2c, I) and the subsequent photoinduced electron transfer from methanol to TiO_2 continues even in the presence of M_n on the surface. The proton and electron also migrate to M_n (Fig. 2c, II), generating the hydrogen-adsorbed M_n and the TiO_2-bound methoxy group (Fig. 2c, III). The subsequent hydrogen atom abstraction from the TiO_2-bound methoxy group continues (Fig. 2c, III), leading to the formation of dihydrogen-adsorbed M_n and formaldehyde-adsorbed TiO_2 (Fig. 2c, IV). The fresh M_n–TiO_2 is regenerated by desorption of hydrogen and formaldehyde (Fig. 2c, V). Likewise, methanediol (Fig. 2d, I), formic acid (Fig. 2d, II), and methoxymethanol (Fig. 2d, III) also produce hydrogen and the corresponding dehydrogenated products. We suggest that the same principle applies to the recently reported photocatalytic dehydrogenation from the electron richer benzyl alcohol and isopropanol with M_n–TiO_2 [88,89]. The mechanisms for the photocatalytic hydrolyses of MF and DMM and photocatalytic decompositions of MF, in particular R_{14}, are not clear at this stage.

The fact that the dehydrogenation reactions in Scheme 1 are the rate-determining steps coincides with the literature reports that hydrogen abstraction is most difficult [73,74,90]. Although future studies are necessary to confirm the details of the mechanism, the unambiguous formation of CT complexes between the organic donors and TiO_2 surface and the requirement of photoirradiation for the overall reaction ensure that the photoinduced electron transfer triggers the reaction. Because the CT bands appear in the 200–400 nm region, the photoinduced electron transfer is expected to be driven by the UV part of the solar simulated light (SI-6). The measured quantum yields indeed show that the photoreaction becomes active at the wavelengths below 400 nm, reaching 13% at 365 nm (SI-7).

6. Discussion from the aspect of one-pot AP

The scheme of the fifteen reactions (Scheme 1) shows that the dead-end products that escape from the cyclic reactions are CO_2, H_2, DME, CH_4, and CO through the reactions of R_5, R_{11}, R_{13}, and R_{15}. Under the condition where the methanol concentration is low, the bimolecular reactions R_4 and R_6 would be suppressed, making the dehydrogenation pathways R_2, R_3, and R_5 become dominant. Thus, if small amounts of methanol were indeed produced under the one-pot AP conditions, it will be quickly decomposed to 3 H_2 and CO_2.

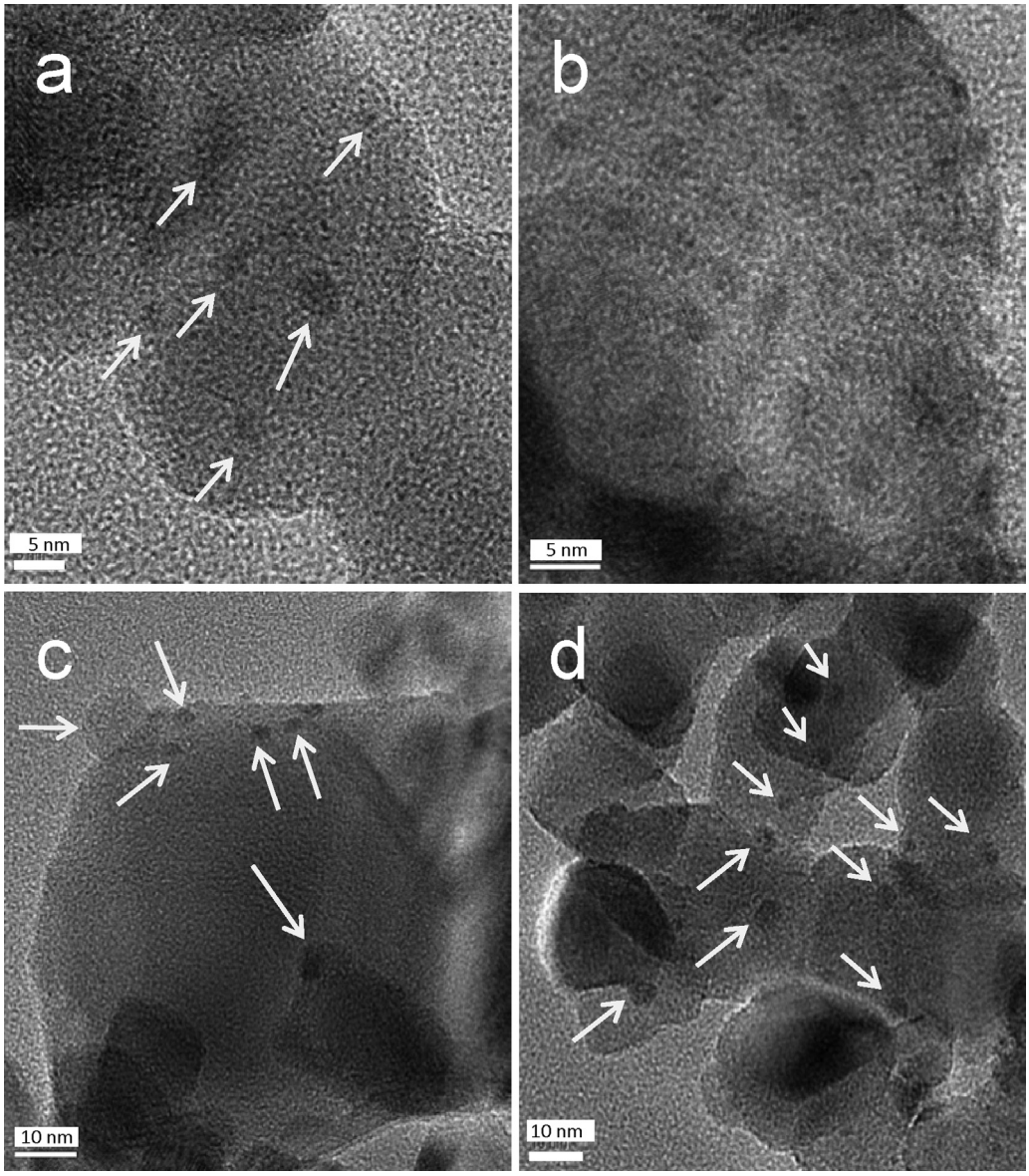

Fig. 3. TEM images of $(MO)_n$–TiO_2 showing the $(MO)_n$ particles. (a) $(PdO)_n$–TiO_2, (b) $(PtO)_n$–TiO_2, (c) $(AuO)_n$–TiO_2, (d) $(CuO)_n$–TiO_2.

However, no one-pot AP systems with M_n–TiO_2 as photocatalysts have ever showed the production of H_2 as the major products, indicating that methanol, formaldehyde, and formic acid have not been produced under such reaction conditions.

CH_4 and CO are also not likely to be produced from the unimolecular decompositions of methyl formate (R_{15} and R_{13}), due to the low concentration of methanol, which suppresses esterification of methanol and formic acid (R_4) to methyl formate, and due to the fact that CH_4 and CO are formed from methyl formate only under the dry condition. Furthermore, under the dry condition, the rate of homolysis to two formaldehyde (rR_{14}) is faster than the two heterolysis pathways by about 140 times (*vide supra*). This means that even if methyl formate was produced, it would be converted to formaldehyde which will subsequently undergo R_2 and R_3, giving rise to the eventual formation of 3 H_2 and CO_2, under such a very low methanol concentration condition arising from the very low efficiency of one-pot AP systems.

Based on the above, we raise a strong doubt to the pathways that have been proposed in the literature for the production of CH_4 as the major product, namely, formaldehyde [44,45], carbine [20a,46–50], and glyoxal [51–53] pathways, because these pathways all involve methanol, formaldehyde and formic acid, in part or as a whole, as the intermediate(s) or as the side product. We therefore propose that CH_4 and CO should be produced directly from the photocatalysts via still non-elucidated pathways but not via formation of methanol, formaldehyde, and formic acid.

This conclusion also clearly indicates that one should no longer expect to obtain formic acid, formaldehyde, and methanol from the one-pot AP systems, in particular with M_n–TiO_2 as photocatalysts, under the condition of one sun, 1 bar of CO_2, and neutral or slightly acid condition. In this regard, the observation of methanol and formaldehyde by the use of very high CO_2 pressure (>10–75 bar) [34–36], deep UV (254, and $\lambda > 280$ nm) [18,21–26] highly basic aqueous solution (pH > 13) [37–39], and very strong sun light (20–100 sun) [40] should receive special attention.

Methanol and various organic bases have been extensively used as the sacrificial reagents as hole scavengers during the tests of photocatalysts for production of hydrogen from water [91–93]. Our result further shows that hydrogen can be produced more easily from the organic sacrifices than water. In this sense, we propose that the reported photocatalysts whose catalytic efficiencies have been evaluated by this methodology should be reevaluated

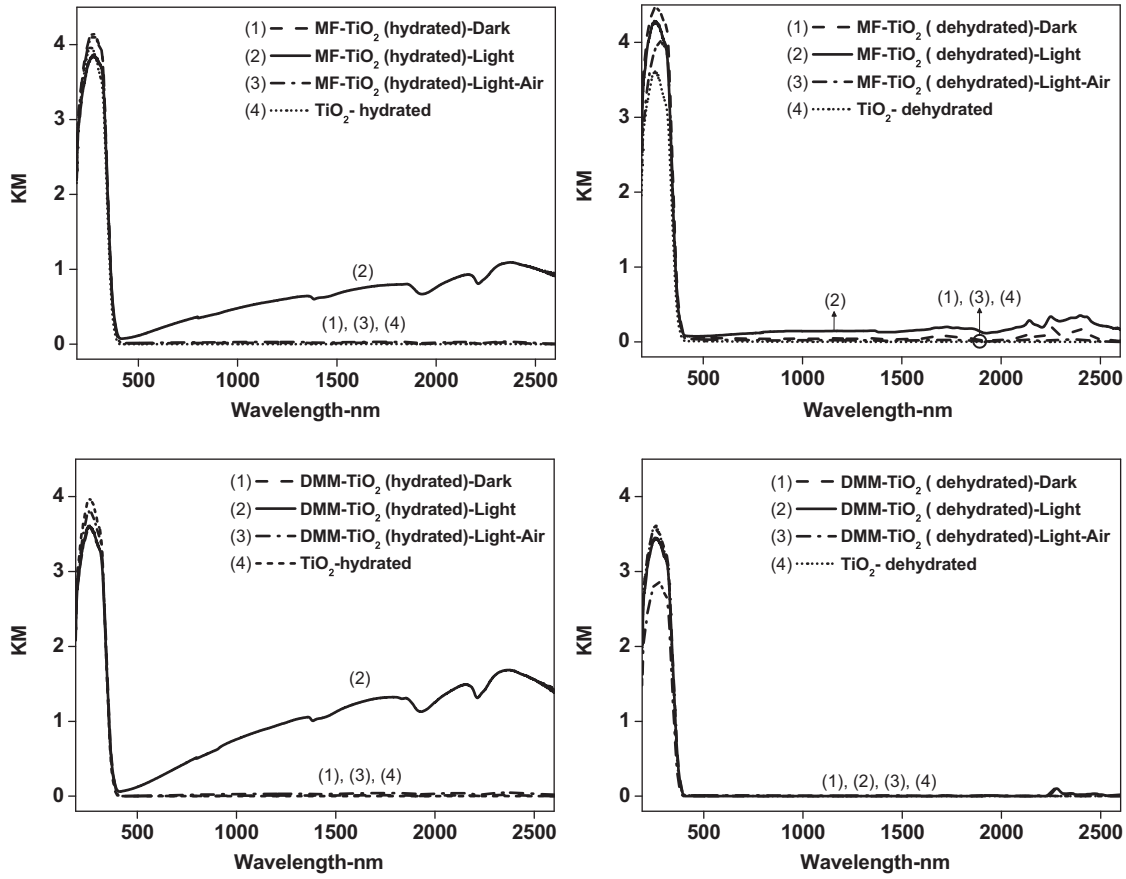

Fig. 4. The diffuse reflectance spectra of hydrated (left) and dehydrated (right) TiO_2 adsorbed with MF (top) and DMM (bottom), respectively, before and after irradiation.

regarding their real efficiencies. One also should keep this point in mind during the evaluation of the catalytic efficiencies of newly developed photocatalysts. In fact, the pathway for the production of hydrogen from methanol has been discussed in depth in the literature [94,95]. For this, the free radical mechanism involving hydroxyl radical (·OH) and hydroxyl methyl radical ($\cdot CH_2OH$) has often been accepted.

We propose that it is difficult for the above free radical pathway to become the major route for the dehydrogenation of methanol because this mechanism involves highly unstable free radicals such as hydroxyl and hydroxymethyl radicals. This mechanism is not realistic because this involves the formation of hydroxyl radical despite the fact that there are electron richer organic donors such methanol and other higher alcohols. Nevertheless this free radical pathway may undergo as a high energy alternative when the one-pot AP systems are irradiated with deep UV light with wavelength shorter than 350 nm in particular with those that are shorter than 300 nm (such as 254, 280, and 290 nm) which can produce highly energetic holes within TiO_2. Indeed, Anpo and the coworkers observed the formation of Ti(III) centers, H and CH_3 radicals during the reduction of CO_2 with H_2O on Cu/TiO2 with UV [20d]. Thus we propose the low energy CT pathway described in Fig. 2 is the most reasonable especially when the irradiation wavelengths are longer than 350 nm.

7. Discussion from the aspect of photocatalytic production of useful compounds

As have been discussed (*vide supra*), some of the fifteen reactions described in Scheme 1 can be rephrased as methanol steam reforming [70–72], dehydrogenation of methanol to formaldehyde or formic acid [73,82,83,96], autooxidation of formaldehyde to carbon dioxide and water [54,75,76], decomposition of formic acid to hydrogen and carbon dioxide [78–80], oxidative coupling of methanol to methyl formate (MF) [74,97–103], and dimethoxymethane (DMM) [104,105], hydrolysis of MF to methanol and formic acid [106], decomposition of dry MF to formaldehyde and other compounds [68,69], and hydrolysis of DMM to methanol and formaldehyde [107,108]. These reactions are in fact currently receiving great attention because they are related to the production of hydrogen from methanol and formic acid, the removal of harmful formaldehyde vapor from the indoor and outdoor atmospheres, and the production of useful compounds such as MF, dry formaldehyde, and DMM from methanol. In this respect, various thermocatalysts have been developed for the above reactions and elucidations of their mechanisms have been conducted. However, the highly efficient photocatalytic pathways and the universal yet cheap photocatalysts which enable all of the above reactions have not been developed, despite the fact that such pathways and catalysts would be an important addition to the above field from the academic and industrial points of view. In that respect, this work not only gives insights into the processes by which methane and carbon monoxide are formed as the major products from the one-pot AP systems with M_n–TiO_2 as photocatalysts, but also reveals the important fact that M_n–TiO_2 are cheap yet highly useful universal photocatalysts which enable all of the above reactions [109].

8. Conclusion

Methanol, formaldehyde, and formic acid are not produced from the one-pot AP systems charged with M_n–TiO_2 (M = Pd, Pt, Cu and

Au) as catalysts under normal conditions (1 bar of CO_2, 1 sun, neutral condition, and the irradiation wavelength > 350 nm). This result raises a doubt on the formaldehyde, carbene, and glyoxal pathways, which have been proposed in the literature to explain the appearance of CH_4 as the major product in such AP systems, because these pathways all involve methanol, formaldehyde, and formic acid, in part or as a whole, as the intermediate(s) or as the side product. This result further suggests that CH_4 and CO should be produced directly from the photocatalysts via still non-elucidated pathways. Therefore, one should no longer expect to obtain formic acid, formaldehyde, and methanol from the one-pot AP systems, in particular with M_n–TiO_2 as photocatalysts.

During irradiation of the one-pot AP system with methanol as the added reagent, fifteen different reactions shown in Scheme 1 take place. These reactions can also be used for production of various useful compounds [109]. M_n–TiO_2 serves as cheap yet highly useful universal photocatalysts which enable all of the above reactions. The reaction is initiated by photoinduced excitation of the charge-transfer (CT) band from methanol to TiO_2 surface which appears in the UV region by the UV part of the solar light.

Methanol and various organic bases have been extensively used as the sacrificial reagents as hole scavengers during the tests of photocatalysts for production of H_2 from water. Hydrogen can be produced more easily from the organic sacrifices than water. The reported photocatalysts whose catalytic efficiencies have been evaluated by this methodology should be reevaluated regarding their real efficiencies. This point should be considered during the evaluation of the catalytic efficiencies of newly developed water reduction photocatalysts using organic sacrifices as hole scavengers.

Acknowledgements

We thank the Korea Center for Artificial Photosynthesis (KCAP) located in Sogang University funded by Ministry of Science, ICT and Future Planning through the National Research Foundation of Korea (No. 2009-0093886). We also thank Jiyun Lee for the help to compile various data and to prepare Scheme 1.

Appendix A. Supplementary data

Supplementary data associated with this article can be found, in the online version, at http://dx.doi.org/10.1016/j.cattod.2014.07.056.

References

[1] J.J. Concepcion, R.L. House, J.M. Papanikolas, T.J. Meyer, Proc. Natl. Acad. Sci. U.S.A. 109 (2012) 15560–15564.
[2] D.G. Nocera, Acc. Chem. Res. 45 (2012) 767–776.
[3] M.D. Kärkäs, E.V. Johnston, O. Verho, B. Åkermark, Acc. Chem. Res. 47 (2013) 100–111.
[4] D. Gust, T.A. Moore, A.L. Moore, Acc. Chem. Res. 42 (2009) 1890–1898.
[5] S. Styring, Faraday Discuss. 155 (2012) 357–376.
[6] (a) S. Haussener, C. Xiang, J.M. Spurgeon, S. Ardo, N.S. Lewis, A.Z. Weber, Energy Environ. Sci. 5 (2012) 9922–9935;
(b) M.G. Walter, E.L. Warren, J.R. Mckone, S.W. Boettcher, Q. Mi, E.A. Santori, N.S. Lewis, Chem. Rev. 110 (2010) 6446–6473;
(c) N.S. Lewis, D.G. Nocera, Proc. Natl. Acad. Sci. U.S.A. 103 (2006) 15729–15735.
[7] M.R. Wasielewski, Chem. Rev. 92 (1992) 435–461.
[8] (a) F. Jiao, H. Frei, Angew. Chem. Int. Ed. 48 (2009) 1841–1844;
(b) W. Lin, H. Frei, J. Am. Chem. Soc. 127 (2005) 1610–1611.
[9] J. Barber, Chem. Soc. Rev. 38 (2009) 185–196.
[10] K. Kalyanasundaram, M. Graetzel, Curr. Opin. Biotechnol. 21 (2010) 298–310.
[11] T.A. Faunce, W. Lubitz, A.W. Rutherford, D. MacFarlane, G.F. Moore, P. Yang, D.G. Nocera, T.A. Moore, D.H. Gregory, S. Fukuzumi, K.B. Yoon, F.A. Armstrong, M.R. Wasielewski, S. Styring, Energy Environ. Sci. 6 (2013) 695–698.
[12] P. Yang, Mater. Res. Soc. Bull. 37 (2012) 806–810.
[13] S. Fukuzumi, Phys. Chem. Chem. Phys. 10 (2008) 2283–2297.
[14] (a) K. Sekizawa, K. Maeda, K. Domen, K. Koike, O. Ishitani, J. Am. Chem. Soc. 135 (2013) 4596–4599;
(b) S. Sato, T. Morikawa, T. Kajino, O. Ishitani, Angew. Chem. 125 (2013) 1022–1026.
[15] A.M. Appel, J.E. Bercaw, A.B. Bocarsly, H. Dobbek, D.L. Dubois, M. Dupuis, J.G. Ferry, E. Fujita, R. Hille, P.J.A. Kenis, C.A. Kerfeld, R.H. Morris, C.H.F. Peden, A.R. Portis, S.W. Ragsdale, T.B. Rauchfuss, J.N.H. Reek, L.C. Seefeldt, R.K. Thauer, G.L. Waldrop, Chem. Rev. 113 (2013) 6621–6658.
[16] (a) W.H. Wang, J.T. Muckerman, E. Fujita, Y. Himeda, ACS Catal. 3 (2013) 856–860;
(b) J. Schneider, H. Jia, J.T. Muckerman, E. Fujita, Chem. Soc. Rev. 41 (2012) 2036–25051.
[17] K. Xie, N. Umezawa, N. Zhang, P. Reunchan, Y. Zhang, J. Ye, Energy Environ. Sci. 4 (2011) 4211–4219.
[18] T. Inoue, A. Fujishima, S. Konishi, K. Honda, Nature 277 (1979) 637–638.
[19] (a) S.N. Habisreutinger, L. Schmidt-Mende, J.K. Stolarczyk, Angew. Chem. Int. Ed. 52 (2013) 7372–7408;
(b) N.M. Dimitrijevic, I.A. Shkrob, D.J. Gosztola, T. Rajh, J. Phys. Chem. C 116 (2012) 878–885.
[20] (a) H. Yamashita, Y. Fujii, Y. Ichihashi, S.G. Zhang, K. Ikeue, D.R. Park, K. Koyano, T. Tatsumi, M. Anpo, Catal. Today 45 (1998) 221–227;
(b) K. Ikeue, S. Nozaki, M. Ogawa, M. Anpo, Catal. Lett. 80 (2002) 111–114;
(c) M. Anpo, H. Yamashita, Y. Ichihashi, Y. Fujii, M. Honda, J. Phys. Chem. B 101 (1997) 2632–2726;
(d) H. Yamashita, H. Nishiguchi, N. Kamada, M. Anpo, Y. Teraoka, H. Hatano, S. Ehara, K. Kikui, L. Palmisano, A. Sclafani, M. Schiavello, M.A. Fox, Res. Chem. Intermed. 20 (1994) 815–823;
(e) M. Anpo, H. Yamashita, K. Ikeue, S.G. Zhang, Y. Ichihashi, D.R. Park, Y. Suzuki, K. Koyano, T. Tatsumi, J. Phys. Chem. B 101 (1997) 2632–2636.
[21] (a) W.N. Wang, W.J. An, B. Ramalingam, S. Mukherjee, D.M. Niedzwiedzki, S. Gangopadhyay, P. Biswas, J. Am. Chem. Soc. 134 (2012) 11276–11281;
(b) W.N. Wang, J. Park, P. Biswas, Catal. Sci. Technol. 1 (2011) 593–600.
[22] W. Hou, W.H. Hung, P. Pavaskar, A. Goeppert, M. Aykol, S.B. Cronin, ACS Catal. 1 (2011) 929–936.
[23] J. Pan, X. Wu, L. Wang, G. Liu, G.Q. Lu, H.M. Cheng, Chem. Commun. 47 (2011) 8361–8363.
[24] T. Yui, A. Kan, C. Saitoh, K. Koike, T. Ibusuki, O. Ishitani, ACS Appl. Mater. Interfaces 3 (2011) 2594–2600.
[25] W. Kim, T. Seok, W. Choi, Energy Environ. Sci. 5 (2012) 6066–6070.
[26] M. Tahir, N.S. Amin, Appl. Catal., A: Gen. 467 (2013) 483–496.
[27] (a) T.W. Woolerton, S. Sheard, E. Pierce, S.W. Ragsdale, F.A. Armstrong, Energy Environ. Sci. 4 (2011) 2393–2399;
(b) T.W. Woolerton, S. Sheard, E. Reisner, E. Pierce, S.W. Ragsdale, F.A. Armstrong, J. Am. Chem. Soc. 132 (2010) 2132–2133.
[28] Q. Zhang, Y. Li, E.A. Ackerman, M.G. Josifovska, H. Li, Appl. Catal., A: Gen. 400 (2011) 195–202.
[29] Y.T. Liang, B.K. Vijayan, K.A. Gray, M.C. Hersam, Nano Lett. 11 (2011) 2865–2870.
[30] C. Wang, R.L. Thompson, J. Baltrus, C. Matranga, J. Phys. Chem. Lett. 1 (2010) 48–53.
[31] O.K. Varghese, M. Paulose, T.J. LaTempa, C.A. Grimes, Nano Lett. 9 (2009) 731–737.
[32] J.Z.Y. Tan, Y. Fernandez, D. Liu, M. Maroto-Valer, J. Bian, X. Zhang, Chem. Phys. Lett. 531 (2012) 149–154.
[33] X. Li, Z. Zhuang, W. Li, H. Pan, Appl. Catal., A: Gen. 429 (2012) 31–38.
[34] S. Xie, Y. Wang, Q. Zhang, W. Fan, W. Deng, Y. Wang, Chem. Commun. 49 (2013) 2451–2453.
[35] T. Mizuno, K. Adachi, K. Ohta, A. Saji, J. Photochem. Photobiol. A: Chem. 98 (1996) 87–90.
[36] M.A. Asi, C. He, M. Su, D. Xia, L. Lin, H. Deng, Y. Xiong, R. Qiu, X.Z. Li, Catal. Today 175 (2011) 256–263.
[37] (a) H.C. Yang, H.Y. Lin, Y.S. Shien, J.C.S. Wu, H.H. Wu, Catal. Lett. 131 (2009) 381–387;
(b) I.H. Tseng, J.C.S. Wu, H.Y. Chou, J. Catal. 221 (2004) 432–440.
[38] (a) Z.H. Zhao, J.M. Fan, Z.Z. Wang, J. Clean. Prod. 15 (2007) 1894–1897;
(b) D. Luo, Y. Bi, W. Kan, N. Zhang, S. Hong, J. Mol. Struct. 994 (2011) 325–331.
[39] (a) S. Krejcikova, L. Matejova, K. Koci, L. Obalova, Z. Matej, L. Capek, O. Solcova, Appl. Catal., B: Environ. 111–112 (2012) 119–125;
(b) J. Mao, T. Peng, X. Zhang, K. Li, L. Zan, Catal. Commun. 28 (2012) 38–41.
[40] (a) J.C.S. Wu, Catal. Surv. Asia 13 (2009) 30–40;
(b) T.V. Nguyen, J.C.S. Wu, Appl. Catal. A: Gen. 335 (2008) 112–120.
[41] (a) Q. liu, Y. Zhou, J. Kou, X. Chen, Z. Tian, J. Gao, S. Yan, Z. Zou, J. Am. Chem. Soc. 132 (2010) 14385–14387;
(b) S. Cheng, S.X. Ouyang, J. Gao, M. Yang, J.Y. Feng, X.X. Fan, L.J. Wan, Z.S. Li, J.H. Ye, Y. Zhou, Z.G. Zou, Angew. Chem. Int. Ed. 49 (2010) 6400–6404.
[42] O. Kozák, P. Praus, K. Koći, M. Klementová, J. Colloid Interface Sci. 352 (2010) 244–251.
[43] F. Sastre, A. Corma, H. Garcia, J. Am. Chem. Soc. 134 (2012) 14137–14141.
[44] M. Subrahmanyam, S. Kanseo, N. Alonso-Vante, Appl. Catal., B: Environ. 23 (1999) 169–174.
[45] N.M. Dimitrijevic, B.K. Vijayan, O.G. Poluektov, T. Rajh, K.A. Gray, H. He, P. Zapol, J. Am. Chem. Soc. 133 (2011) 3964–3971.
[46] (a) K. Mori, H. Yamashita, M. Anpo, RSC Adv. 2 (2012) 3165–3172;
(b) K. Ikeue, S. Nozaki, M. Ogawa, M. Anpo, Catal. Today 74 (2002) 241–248.
[47] N. Sasirekha, S.J.S. Basha, K. Shanthi, Appl. Catal., B: Environ. 62 (2006) 169–180.

[48] S.S. Tan, L. Zou, E. Hu, Catal. Today 131 (2008) 125–129.
[49] I.A. Shkrob, N.M. Dimitrijevic, T.W. Marin, H. He, P. Zapol, J. Phys. Chem. C 116 (2012) 9461–9471.
[50] H. He, P. Zapol, L.A. Curtiss, Energy Environ. Sci. 5 (2012) 6196–6205.
[51] G.R. Dey, A.D. Belapukar, K. Kishore, J. Photochem. Photobiol. A: Chem 163 (2004) 503–508.
[52] G.R. Dey, K.K. Pushpa, Res. Chem. Intermed. 33 (2007) 631–641.
[53] S. Sato, J. Phys. Chem. 87 (1983) 3531–3537.
[54] T. Salthammer, Angew. Chem. Int. Ed. 52 (2013) 3320–3327.
[55] S. Izadyar, S.F. Fatemi, Ind. Eng. Chem. Res. 52 (2013) 10961–10968.
[56] N. Roy, Y. Sohn, D. Pradhan, ACS Nano 7 (2013) 2532–2540.
[57] R. Chalasani, S. Vasudevan, ACS Nano 7 (2013) 4093–4104.
[58] S. Kitano, N. Murakami, T. Ohno, Y. Mitani, Y. Nosaka, H. Asakura, K. Teramura, T. Tanaka, H. Tada, K. Hashimoto, H. Kominami, J. Phys. Chem. C 117 (2013) 11008–11016.
[59] W.J. Lee, J.M. Lee, S.T. Kochuveedu, T.H. Han, H.Y. Jeong, M. Park, J.M. Yun, J. Kwon, K. No, D.H. Kim, S.O. Kim, ACS Nano 6 (2012) 935–943.
[60] X. Qiu, M. Miyauchi, K. Sunada, M. Minoshima, M. Liu, Y. Lu, D. Li, Y. Shimodaira, Y. Hosogi, Y. Kuroda, K. Hashimoto, ACS Nano 6 (2012) 1609–1618.
[61] R. Su, R. Tiruvalam, Q. He, N. Dimitratos, L. Kesavan, C. Hammond, J.A. Lopez-Sanchez, C.J. Kiely, G.J. Hutchings, F. Besenbacher, ACS Nano 6 (2012) 6284–6292.
[62] H. Chen, Y. Xu, J. Phys. Chem. C 116 (2012) 24582–24589.
[63] H. Li, S. Yin, Y. Wang, T. Sato, Environ. Sci. Technol. 46 (2012) 7741–7745.
[64] Y. Wang, Y. Zhang, G. Zhao, H. Tian, H. Shi, T. Zhou, ASC Appl. Mater. Interfaces 4 (2012) 3965–3972.
[65] A.A. Ismail, D.W. Bahnemann, S.A. Al-Sayari, Appl. Catal., A: Gen. 431 (2012) 62–68.
[66] Z. Niu, Y.R. Zhen, M. Gong, Q. Peng, P. Nordlander, Y. Li, Chem. Sci. 2 (2011) 2392–2395.
[67] N. Matubayasi, S. Morooka, M. Nakahara, H. Takahashi, J. Mol. Liq. 134 (2007) 58–63.
[68] J.S. Francisco, J. Am. Chem. Soc. 125 (2003) 10475–10480.
[69] W.K. Metcalfe, J.M. Simmie, H.J. Curran, J. Phys. Chem. A 114 (2010) 5478–5484.
[70] M. Kusche, F. Enzenberger, S. Bajus, H. Niedermeyer, A. Bösmann, A. Kaftan, M. Laurin, J. Libuda, P. Wasserscheid, Angew. Chem. Int. Ed. 52 (2013) 5028–5032.
[71] K.M.K. Yu, W. Tong, A. West, K. Cheung, T. Li, G. Smith, Y. Guo, S.C.E. Tsang, Nat. Commun. 3 (2014) 1230–1237.
[72] D.R. Palo, R.A. Dagle, J.D. Holladay, Chem. Rev. 107 (2007) 3392–4021.
[73] Q. Guo, C. Xu, Z. Ren, W. Yang, Z. Ma, D. Dai, H. Fan, T.K. Minton, X. Yang, J. Am. Chem. Soc. 134 (2012) 13366–13373.
[74] Q. Yuan, Z. Wu, Y. Jin, L. Xu, F. Xiong, F. Ma, W. Huang, J. Am. Chem. Soc. 135 (2013) 5212–5219.
[75] X. Chen, H.Y. Zhu, J.C. Zhao, Z.F. Zheng, X.P. Gao, Angew. Chem. Int. Ed. 47 (2008) 5336–5353.
[76] C. Zhang, F. Liu, Y. Zhai, H. Ariga, N. Yi, Y. Liu, K. Asakura, M. Flytzani-Stephanopolous, H. He, Angew. Chem. Int. Ed. 51 (2012) 9628–9632.
[77] S. Kakuta, T. Abe, Appl. Mater. Interfaces 1 (2009) 2707–2710.
[78] S. Zhang, Ö. Metin, D. Su, S. Sun, Angew. Chem. Int. Ed. 51 (2013) 3681–3684.
[79] (a) X. Gu, Z.H. Lu, H.L. Jiang, T. Akita, Q. Xu, J. Am. Chem. Soc. 133 (2011) 11822–11825;
(b) Z.L. Wang, J.M. Yan, Y. Ping, H.L. Wang, W.T. Zheng, Q. Jiang, Angew. Chem. Int. Ed. 52 (2013) 4406–4409.
[80] A. Boddien, D. Mellmann, F. Gärtner, R. Jackstell, H. Junge, P.J. Dyson, G. Laurenczy, R. Ludgwin, M. Beller, Science 333 (2011) 1733–1736.
[81] Y. Fu, H. Zhu, J. Shen, Thermochim. Acta 434 (2005) 88–92.
[82] S. Su, P. Zaza, A. Renken, Chem. Eng. Technol. 17 (1994) 34–40.
[83] L.P. Ren, W. Dai, Y. Cao, H. Li, K. Fan, Chem. Commun. 24 (2003) 3030–3031.
[84] T. Tachikawa, S. Tojo, M. Fujitsuka, T. Majima, Langmuir 20 (2004) 2753–2759.
[85] T. Rajh, L.X. Chen, K. Lukas, T. Liu, M.C. Thurnauer, D.M. Tiede, J. Phys. Chem. B 106 (2002) 10543–10552.
[86] N.K. Jeong, J.S. Lee, E.L. Tae, Y.J. Lee, K.B. Yoon, Angew. Chem. Int. Ed. 47 (2008) 10128–10132.
[87] Y.S. Seo, C. Lee, K.H. Lee, K.B. Yoon, Angew. Chem. Int. Ed. 44 (2004) 910–913.
[88] K. Imamura, H. Tsukahara, K. Hamamichi, N. Seto, K. Hashimoto, Appl. Catal., A: Gen. 450 (2013) 28–33.
[89] A. Tanaka, S. Sakaguchi, K. Hashimoto, H. Kominami, ACS Catal. 3 (2013) 79–85.
[90] T. Mallat, A. Baiker, Chem. Rev. 104 (2004) 3037–3058.
[91] X. Chen, L. Liu, P.Y. Yu, S.S. Mao, Science 331 (2011) 746–749.
[92] D. Wang, A. Pierre, Md.G. Kibria, K. Cui, X. Han, H. Han, K.H. Bevan, H. Guo, S. Paradis, A.R. Hakima, Z. Mi, Nano Lett. 11 (2011) 2353–2357.
[93] H. Zhou, E.M. Sabio, T.K. Townsend, T. Fan, D. Zhang, F.E. Osterloh, Chem. Mater. 22 (2010) 3362–3368.
[94] X. Chen, S. Shen, L. Guo, S.S. Mao, Chem. Rev. 110 (2010) 6503–6570.
[95] Y. Li, J. Wang, S. Peng, G. Lu, S. Li, Int. J. Hydrogen Energy 35 (2010) 7116–7126.
[96] M. Nielsen, E. Alberico, W.W. Baumann, H.J. Drexler, H. Junge, S. Gladiali, M. Beller, Nature 495 (2013) 85–89.
[97] A. Wittsock, V. Zielasek, J. Biener, C.M. Friend, M. Bäumer, Science 327 (2010) 319–322.
[98] K.R. Phillips, S.C. Jensen, M. Baron, S.C. Li, C.M. Friend, J. Am. Chem. Soc. 135 (2013) 574–577.
[99] X.R. Liu, J. Madix, C.M. Friend, Chem. Rev. 37 (2008) 2243–2261.
[100] B. Xu, X. Liu, J. Haubrich, R.J. Madix, C.M. Friend, Angew. Chem. Int. Ed. 48 (2009) 4206–4209.
[101] B. Xu, X. Liu, J. Haubrich, C.M. Friend, Nat. Chem. 2 (2010) 61–65.
[102] J. Liu, E. Zhan, W. Cai, J. Li, W. Shen, Catal. Lett. 120 (2008) 274–280.
[103] W. Li, W. Liu, E. Iglesia, J. Phys. Chem. B 110 (2006) 23337–23342.
[104] J. Gornay, X. Sécordel, G. Tesuet, B.D. Ménorval, S. Cristol, P. Fongarland, M. Capron, L. Duhamel, E. Payen, J.L. Dubois, F. Dumeignil, Green Chem. 12 (2010) 1722–1725.
[105] O. Nikonova, M. Capron, G. Fang, J. Faye, A.S. Mamede, L.J. Duhamel, F. Dumeignil, G.A. Seisenbaeva, J. Catal. 279 (2011) 310–318.
[106] O. Jogunala, T. Salmi, J. Wärnå, J.P. Mikkola, E. Tirronen, Ind. Eng. Chem. Res. 50 (2011) 267–276.
[107] H. Shen, Y. Fu, Q. Sun, S. Zho, A. Auroux, J. Shen, Catal. Commun. 9 (2008) 806–810.
[108] Y. Fu, J. Shen, J. Catal. 248 (2007) 101–110.
[109] A.R. Koirala, S. Docao, K.B. Yoon, RSC Adv. 4 (2014) 33144–33148.